

1 **Reassessing seasonal sea ice predictability of the Pacific-Arctic sector using**
2 **a Markov model**

3 Yunhe Wang^{1,4}, Xiaojun Yuan², Haibo Bi^{1,3,4}, Mitchell Bushuk⁵, Yu Liang^{1,6},
4 Cuihua Li², Haijun Huang^{1,3,4,6}

5 ¹ CAS Key Laboratory of Marine Geology and Environment, Institute of Oceanology,
6 Chinese Academy of Sciences, Qingdao, China.

7 ² Lamont-Doherty Earth Observatory of Columbia University, New York, USA.

8 ³ Laboratory for Marine Geology, Qingdao National Laboratory for Marine Science
9 and Technology, Qingdao, China.

10 ⁴ Center for Ocean Mega-Science, Chinese Academy of Sciences, Qingdao, China.

11 ⁵ National Oceanic and Atmospheric Administration/Geophysical Fluid Dynamics
12 Laboratory, Princeton, New Jersey, USA

13 ⁶ University of Chinese Academy of Sciences, Beijing, China

14 Corresponding author: Xiaojun Yuan (xyuan@ldeo.columbia.edu)

15 **Abstract**

16 In this study, a regional linear Markov model is developed to assess seasonal sea ice
17 predictability in the Pacific-Arctic sector. Unlike an earlier pan-Arctic
18 Markov model that was developed with one set of variables for all seasons, the
19 regional model consists of four seasonal modules with different sets of predictor
20 variables, accommodating seasonally-varying driving processes. A series of
21 sensitivity tests are performed to evaluate the predictive skill in cross-validated
22 experiments and to determine the best model configuration for each season. The
23 prediction skill, as measured by the sea ice concentration (SIC) anomaly correlation
24 coefficient (ACC) between predictions and observations~~the percentage of grid points~~
25 ~~with significant correlations (PGS)~~, increased by 3275% in the Bering Sea and 186%
26 in the Sea of Okhotsk relative to the pan-Arctic model. The regional Markov model's
27 skill is also superior to the skill of an anomaly persistence forecast. ~~Sea ice~~
28 ~~concentration (SIC)~~ trends significantly contribute to the model skill. However, the
29 model retains skill for detrended sea ice extent predictions up to 76 month lead times
30 in the Bering Sea and the Sea of Okhotsk. We find that subsurface ocean heat content
31 (OHC) provides a crucial source of prediction skill in all seasons, especially in the
32 cold season, and adding sea ice thickness (SIT) to the regional Markov model has a
33 substantial contribution to the prediction skill in the warm season but a negative
34 contribution in the cold season, ~~surface radiative fluxes contribute to predictability in~~
35 ~~the cold season and geopotential height and winds play an indispensable role in the~~
36 ~~warm season forecast, contrasting to the thermodynamic processes dominating the~~
37 ~~pan-Arctic predictability~~. The regional model can also capture the seasonal
38 reemergence of predictability, which is missing in the pan-Arctic model.

39 1 Introduction

40 Sea ice acts as a major component of the Arctic climate system through
41 modulating the radiative flux, heat, and momentum exchanges between the ocean and
42 the atmosphere (Peterson et al., 2017; Porter et al., 2011; Smith et al., 2017). Sea ice
43 also modulates sea surface salinity, which is one of the key drivers for thermohaline
44 circulations (Sévellec et al., 2017). The rapid retreat of Arctic sea-ice extent in the
45 past few decades has been considered a key indicator of climate change (Koenigk et
46 al., 2016; Swart, 2017). The ~~decreasingshrinking~~ Arctic sea ice extent contributes to
47 polar temperature amplification (Kim et al., 2016; Screen and Francis, 2016), an
48 increase in wintertime snowfall over Siberia, northern Canada, and Alaska (Deser et
49 al., 2010), polar stratospheric cooling (Screen et al., 2013; Wu et al., 2016), and
50 potentially contributes to a weakening of the mid-latitude jet (Francis and Vavrus,
51 2012) and increased frequency of cold Northern Hemisphere midlatitude winter
52 events (Cohen et al., 2020; Meleshko et al., 2018).

53 ~~Also, †~~The rapid retreat of summer Arctic sea ice extent ~~retreat~~ has also created
54 more commercial opportunities in the newly opened Arctic waters. The Northwest
55 Passage (through northern Canada) and the Northern Sea Route (north of Russia)
56 could offer faster and less expensive shipping between the Pacific and Atlantic (Smith
57 and Stephenson, 2013). Information on the Arctic marine accessibility and ice-free
58 season duration in the marginal ice zone would enable planning of merchant shipping,
59 conservation efforts, resource extraction, and fishing activities. The growing polar
60 ecotourism industry could also benefit from shrinking sea-ice cover. Therefore,
61 increased efforts have been devoted to developing Arctic sea-ice forecast systems in
62 recent decades.–

63 Substantial efforts have gone toward developing both statistical and dynamical sea
64 ice prediction models. Dynamic models numerically solve equations that govern the
65 sea ice physics using sea-ice, ocean, and/or atmospheric conditions to initialize the
66 models for each season (Bushuk et al., 2019; Bushuk et al., 2020; Bushuk et al., 2021;
67 Dai et al., 2020; Msadek et al., 2014). Numerous studies using fully coupled general

68 circulation models (GCMs) have quantified the seasonal prediction skill of pan-Arctic
69 sea ice extent (SIE), ~~which and~~ have found forecast skill for detrended pan-Arctic
70 SIE at lead times of 1 to 6 months (Blanchard-Wrigglesworth et al., 2015; Day et al.,
71 2014b; Guemas et al., 2016a; Peterson et al., 2015; Sigmond et al., 2013). Bushuk et
72 al. (2017a) evaluated regional Arctic sea ice prediction skill in a Geophysical Fluid
73 Dynamics Laboratory (GFDL) seasonal prediction system. They found skillful
74 detrended ~~regional~~ ~~reigonal~~ SIE predictions, and found that skill varied strongly with
75 both region and season.

76 On the other hand, statistical methods are also appealing for seasonal sea ice
77 predictions (Petty et al., 2017). Statistical models capture relationships between sea
78 ice and oceanic, atmospheric, or time-lagged sea ice predictor. Recently, statistical
79 methods have been used to provide sea ice field predictions using numerous
80 techniques such as linear Markov model (Chen and Yuan, 2004; Yuan et al., 2016),
81 vector autoregressive model (Wang et al., 2019a; Wang et al., 2016), deep neural
82 network (Andersson et al., 2021; Chi and Kim, 2017; Wang et al., 2017), Bayesian
83 logistic regression (Horvath et al., 2020), and the combination of complex networks
84 and Gaussian process regression model (Gregory et al., 2020). In some cases,
85 statistical models provide better performance than dynamical models (Hamilton and
86 Stroeve, 2016). For example, Yuan et al. (2016) showed that a linear Markov model
87 has skillful sea ice concentration (SIC) predictions up to 9-month lead times in many
88 regions of the Arctic and that this statistical model consistently captured more sea ice
89 prediction skill than NOAA/NCEP Climate Forecast System (CFSv2) and the
90 Canadian seasonal and interannual prediction system at the seasonal time scale. The
91 Markov model prediction skill also exhibits strong regional and seasonal dependence.

92 Two common characteristics of sea ice predictability emerged from both dynamic
93 (e.g. CFSv2 and GFDL climate models) and statistical models (e.g. linear Markov
94 models, and linear regression models). First, low prediction skill occurs in the Pacific
95 sector of the Arctic, particularly in the Bering Sea and the Sea of Okhotsk, compared
96 with other Arctic regions (Bushuk et al., 2017a; Yuan et al., 2016). Many factors may

97 lead to this low predictability. Bushuk et al. (2017a) suggest that less persistent sea ice
98 anomalies in the North Pacific sector possibly lead to less predictability in the region
99 by the GFDL dynamical model. The Markov model of Yuan et al. (2016) was built in
100 multivariate empirical orthogonal functions (MEOF) space in the pan-Arctic and the
101 leading modes are dominated by the large long-term trend and strong climate
102 variability in the Atlantic sector (Figure 1). So the signal of sea ice variability in the
103 Pacific sector could be under-represented in the model. Therefore, it is necessary to
104 evaluate the sea ice predictability in the Pacific sector with a new regional model.

105 Second, many studies have shown evidence for an Arctic sea ice spring
106 predictability barrier that causes forecasts initialized prior to May to be less skillful
107 and imposes a relatively sharp limit on regional summer sea ice prediction skill~~low~~
108 ~~predictability occurs in the spring months or is initialized in spring~~ (Bushuk et al.,
109 2017a; Day et al., 2014b; Yuan et al., 2016). Spring sea ice variability is complicated
110 by surface melt ponds. The sea ice driven processes in spring could be different from
111 those in other seasons. The spring barrier may result from a sharp increase in
112 predictability at melt onset, when sea-ice-albedo feedback acts to enhance and persist
113 the preexisting export-generated mass anomaly (Bushuk et al., 2020). ~~In the Pacific~~
114 ~~sector of the Arctic, sea ice does not exist during the summer months in the Bering~~
115 ~~Sea and the Sea of Okhotsk, and sea ice nearly 100% covers the regions within the~~
116 ~~Arctic Basin in winter. Both cases lead to no sea ice variability and therefore no~~
117 ~~predictability. Moreover, the Bering Sea opens to the North Pacific, facing a more~~
118 ~~divergent environment, while sea ice movement is more constrained by the~~
119 ~~geographic setting of the Arctic Basin in the Chukchi Sea, East Siberian Sea, and the~~
120 ~~Beaufort Sea. Strong seasonality and geographic setting dictate that different driving~~
121 ~~processes may play dominant roles in different seasons.~~ In addition, summer
122 initialization months have little sea ice coverage and have little intrinsic memory of
123 sea ice and, therefore, require another source of memory to provide winter SIE
124 prediction skill.

125 Actually, re-emergence mechanisms can provide sources of sea ice predictability
126 on time scales from a few months to 1 year (Blanchard-Wrigglesworth et al., 2011).
127 The re-emergence mechanism mainly relies on the persistence of some sea-ice related

128 variables such as sea ice thickness (SIT) and ocean temperature. Previous studies have
129 shown that summer sea surface temperature (SST) anomalies can provide a significant
130 source of SIE predictability in the ice growth season (Blanchard-Wrigglesworth et al.,
131 2011; Bushuk and Giannakis, 2017; Cheng et al., 2016; Dai et al., 2020). Initializing
132 the upper ocean heat content (OHC) in a seasonal prediction system can also yield
133 remarkable regional skill for winter sea ice (Bushuk et al., 2017a). Moreover,
134 assimilating SIT data can slightly improve the SIC forecast and particularly benefit
135 the sea ice prediction in summer, which is attributed to the long-lived SIT anomalies
136 and their impact on summer sea ice (Blockley and Peterson, 2018; Bushuk et al.,
137 2017b; Guemas et al., 2016b; Xie et al., 2016). Because sea ice is closely coupled
138 with the atmosphere and the ocean, the sea ice predictability is provided by the
139 intrinsic memory of sea ice and its related variables, and accurate initial conditions are
140 of importance for sea ice predictions (Blanchard-Wrigglesworth et al., 2011; Guemas
141 et al., 2016b). Current climate models used for sea ice predictions are usually
142 initialized using various atmospheric and oceanic variables, such as SIC, SIT, OHC,
143 SST, surface air temperature (SAT), or other data from existing reanalysis (Bushuk et
144 al., 2017a; Dai et al., 2020; Kimmritz et al., 2019; Yuan et al., 2016).

145 In this study, we develop a regional linear Markov model for the seasonal
146 prediction of SIC in the Pacific sector with a focus on understanding unique sea ice
147 driving processes in different seasons. We follow the framework of the pan-Arctic
148 linear Markov model (Yuan et al., 2016). Unlike the pan-Arctic model that was
149 developed with one set of variables (SIC, ~~SAT, SST~~surface air temperature, and sea-
150 ~~surface temperature~~) for all seasons and the entire Arctic region, the regional model
151 consists of four modules with seasonal dependent variables, which isolate the
152 dominant processes for each targeted season. Regional relevant predictors are
153 evaluated. New variables, including surface net radiative flux, turbulent heat flux, and
154 pressure and wind fields, as well as SIT and OHC, are introduced to the model
155 experiments. Sea ice predictability is assessed at grid points and over all seasons, and
156 subsequently compared with the pan-Arctic model and other dynamic models.

157 2 Data and methodology

158 2.1 Data

159 Building on the extensive literature studying the predictability and variability of
160 sea ice (Bushuk and Giannakis, 2017; Bushuk et al., 2020; Guemas et al., 2016a;
161 Horvath et al., 2021; Lenetsky et al., 2021; Yuan et al., 2016), we firstly chose many
162 kinds of oceanic and atmospheric variables and examined their correlations with SIC.
163 The results show that SIC is highly related to OHC in the upper 300 m, SIT, SST,
164 SAT, surface net radiative flux, surface net turbulent heat flux, geopotential height
165 and wind vector at different levels including 850 to 200 hPa. Due to the barotropic
166 nature of the polar troposphere (Chen, 2005; Ting, 1994) and the low correlation
167 between sea level pressure and SIC, we chose geopotential height and wind vector at
168 850 hPa to define the low-level atmospheric circulation, whose interaction with sea
169 ice is stronger relative to that in higher levels. Therefore, ~~W~~we choose to define the
170 atmosphere-ice-ocean coupled Arctic climate system with 97 variables: SIC, OHC in
171 the upper 300 m, SIT, ~~sea surface temperature (SST), surface air temperature (SAT),~~
172 surface net radiative flux, surface net turbulent heat flux, 850 hPa geopotential height,
173 and 850 hPa wind vector.

174 Monthly SICs in 25 km × 25 km grids are obtained from the National Snow and
175 Ice Data Center (NSIDC) from 1979 to 2020 (Comiso, 2017). The dataset is generated
176 from brightness temperatures derived from Nimbus-7 Scanning Multichannel
177 Microwave Radiometer (SMMR), Defense Meteorological Satellite Program (DMSP)
178 –F8, -F11, and -F13 Special Sensor Microwave/Imager (SSM/I), and DMSP-F17
179 Special Sensor Microwave Imager/Sounder (SSMIS) using the bootstrap algorithm.
180 Monthly SITs are from the Pan-Arctic Ice-Ocean and Assimilating System (PIOMAS)
181 model data. PIOMAS is a sea ice-ocean reanalysis product that compares reasonably
182 well to available satellite, aircraft, and in situ SIT measurements (Schweiger et al.,
183 2011). The system applies a 12-category SIT and enthalpy distribution (Zhang and
184 Rothrock, 2003) and is driven by NCEP/NCAR reanalysis atmospheric forcing
185 including 10-m surface winds and 2-m SAT.

186 All atmospheric ~~and oceanic~~ variables and SST with a spatial resolution of $1^\circ \times 1^\circ$
187 are from the latest European Centre for Medium-Range Weather Forecasts (ECMWF)
188 reanalysis product ERA5 (Hersbach et al., 2020) and are applied to represent the
189 conditions of the atmosphere and ocean. ERA5 is produced using the version of
190 ECMWF's Integrated Forecast System (IFS), CY41R2, based on a hybrid incremental
191 4D-Var system, with 137 hybrid sigma/pressure (model) levels in the vertical
192 direction, with the top-level at 0.01 hPa. The OHC used here is global ocean and sea-
193 ice reanalysis (ORAS5: Ocean Reanalysis System 5) monthly mean data and is
194 developed by the European Centre for Medium-Range Weather Forecasts (ECMWF)
195 OCEAN5 ocean analysis-reanalysis system (Zuo et al., 2019). ORAS5 includes five
196 ensemble members and covers the period from 1979 onwards. It is regarded as a
197 global eddy-permitting ocean ensemble reanalysis product. Both the forcing fields and
198 observational datasets are updated in ORAS5.

199 **2.2 The model**

200 The idea of using a Markov model for climate prediction is to build multivariate
201 models, aiming to capture the co-variability in the atmosphere-ocean-sea ice coupled
202 system instead of linearly regressing on individual predictors. Yuan et al. (2016)
203 applied this statistical approach to predict SIC in the Arctic at a seasonal timescale
204 and showed that the Lamont statistical model outperformed the NOAA CFSv2
205 operational model and the Canadian Seasonal to Interannual Prediction System in sea
206 ice prediction. They used ~~multivariate empirical orthogonal functions (MEOF)~~ as the
207 building blocks of the model to filter out incoherent small-scale features that are
208 basically unpredictable. Similar Markov models were also developed to study ENSO
209 predictability (Cañizares et al., 2001; Xue et al., 2000) and for East Asian monsoon
210 forecasts (Wu et al., 2013). The success of the Markov model is attributed to the
211 dominance of several distinct modes in the coupled atmosphere-ocean-sea ice system
212 and to the model's ability to pick up these modes.

213 Here we focus on the atmosphere-ocean-sea ice interactive processes that are
214 unique to the Pacific sector and develop a regional linear Markov model for the

215 seasonal prediction of SIC. The model consists of four modules with seasonally
216 dependent variables. The model ~~domainarea~~ extends from 40°N to 84°N in latitude
217 and from 120°E to 240°E in longitude (Figure 1). To reduce model dimensions, we
218 remove land grid cells, mostly open water grid cells and mostly 100% ice cover grid
219 cells from the sea ice field. The mostly open water cells are defined by the grids
220 where SIC \geq 15% only occurred less than 4% of the total all-season time series (492
221 months), and mostly ice covered cells are defined by the grids where SIC \geq 95% for
222 more than 96% of total time series. SIC at the rest grid cells ranges from 0 to 100%.

223 ~~For the sea ice field, the grid cells where the number of months with variable SIC~~
224 ~~(15%–95%) is less than 4% of the total time series (492 months) are masked and~~
225 ~~excluded together with land grid cells.~~— Our model is constructed in the MEOF
226 space. The base functions of the model’s spatial dependence consist of the
227 eigenvectors from the MEOF, while the temporal evolution of the model is a Markov
228 process with its transition functions determined from the corresponding principal
229 components (PCs). We use only several leading MEOF modes, which greatly reduce
230 model space and filter out unpredictable small-scale features. This method of reducing
231 model dimension has been successfully used in earlier Antarctic and Arctic sea ice
232 predictability studies (Chen and Yuan, 2004; Yuan et al., 2016).

233 We preselect SIC, OHC, SIT, SST, SAT, surface net radiative flux, surface net
234 turbulent heat flux, and geopotential height and winds at 850 hPa to represent
235 different sea ice-driving processes in the Pacific sector. We create anomaly time
236 series for all variables from 1979 to 2020 by subtracting climatologies of the same
237 period from monthly mean data. ~~The initial multivariate space is formed to capture the~~
238 ~~predictable variability in the atmosphere-ice-ocean system by MEOF analysis. Since~~
239 ~~our focus is on short term climate variability, the climatological seasonal cycle for the~~
240 ~~period from 1979 to 2020 was subtracted to obtain monthly anomalies for all~~
241 ~~variables.~~ A normalization is applied to the time series at each grid point for all
242 variables. To emphasize sea ice variability in the model construction, we weight SIC
243 by 2 and other variables by 1, although the final model skill is not very sensitive to

244 this choice of weight. The weighted variables are stacked up into a single matrix \mathbf{V} (n,
 245 m), where n is the number of grid points of all fields and m is the length of the time
 246 series. We then decompose \mathbf{V} into eigenvectors (spatial patterns) \mathbf{E} and their
 247 corresponding PCs (time series) \mathbf{P} :

$$248 \quad \mathbf{V} = \mathbf{E}\mathbf{P}^T, \quad (1)$$

249 where the columns of \mathbf{E} are orthogonal and the columns of \mathbf{P} are orthonormal; the
 250 superscript T denotes matrix transpose. It greatly reduces the model space by
 251 truncating (1) to the several leading modes. The Markov model is computed using the
 252 single-step correlation matrix, that is, a transition matrix \mathbf{A} that satisfies the following
 253 linear relation:

$$254 \quad \mathbf{P}_{i+1} = \mathbf{A}\mathbf{P}_i + e_i, \quad (2)$$

255 where i denotes the i th month and e_i is the error in the model fit. Transition \mathbf{A} is
 256 calculated by multiplying (2) with \mathbf{P}_i^T

$$257 \quad \mathbf{P}_{i+1}\mathbf{P}_i^T = \mathbf{A}\mathbf{P}_i\mathbf{P}_i^T + e_i\mathbf{P}_i^T, \quad (3)$$

258 For the best model fit, e_i and \mathbf{P}_i^T should have no correlation. Thus

$$259 \quad \mathbf{A} = (\mathbf{P}_{i+1}\mathbf{P}_i^T)(\mathbf{P}_i\mathbf{P}_i^T)^{-1}. \quad (4)$$

260 \mathbf{A} is constructed to be seasonally-dependent because of the strong seasonality of SIC
 261 and related variables. Thus (4) is applied to 12 subsets of PCs to obtain different
 262 transition matrices for each of the 12 calendar months.

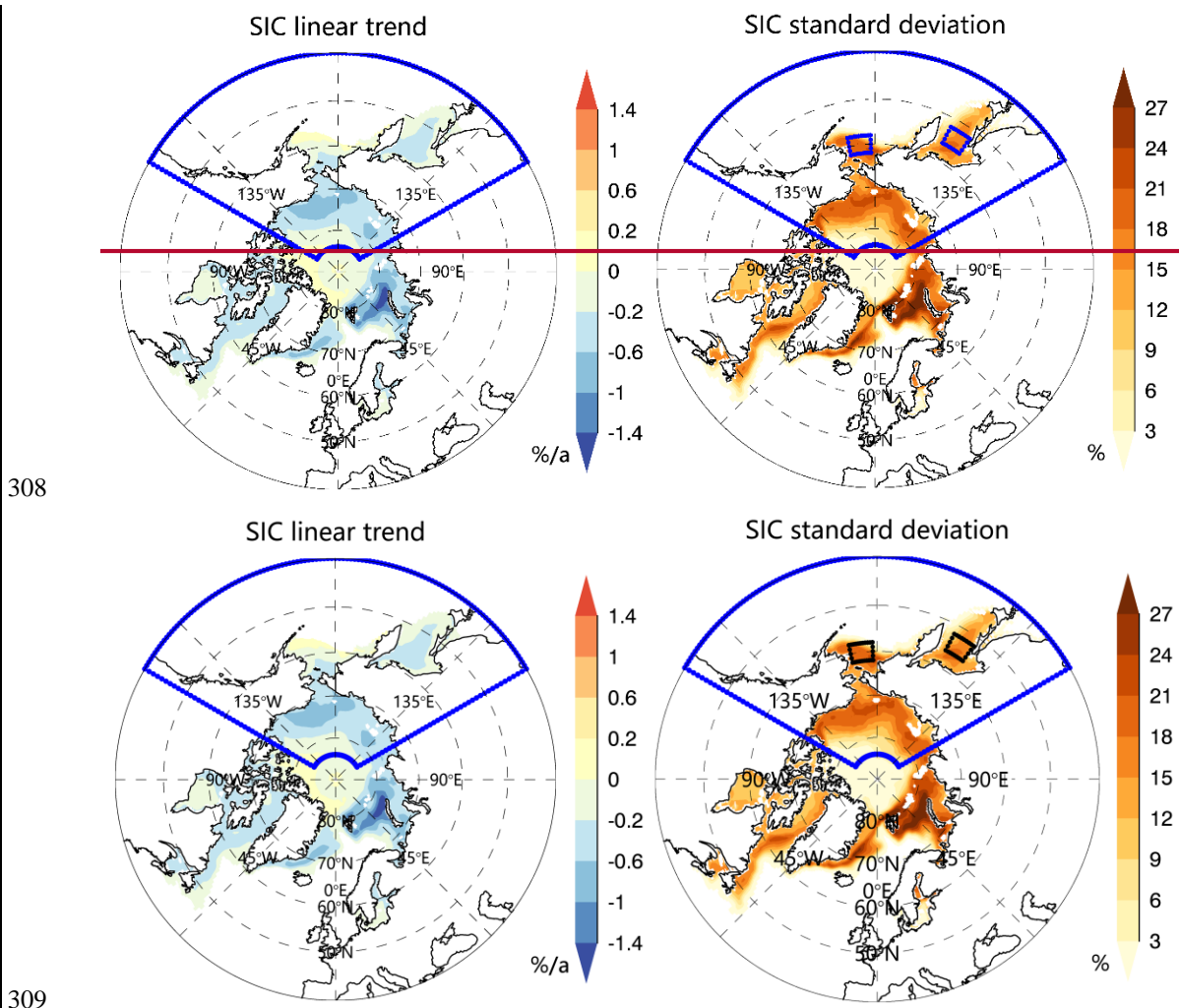
263 After the Markov model is formulated, the SIC prediction can be ~~generated~~made
 264 through the following eight steps: 1) to examine which variables have the highest
 265 prediction potential in the Pacific sector, we create 10 climate variable combinations
 266 representing different driving processes. 2) The PCs corresponding to each initial
 267 multivariate space are calculated by the MEOF equation (1). 3) Transition matrices,
 268 \mathbf{A} , for each calendar month are calculated by equation (4). 4) The predictions of the
 269 PCs are made by truncating to the first several modes and applying the appropriate
 270 transition matrices at different lead times. “Lead time” refers to the number of months

271 prior to the target month that the forecast was initialized. For example, lead-1
272 prediction of January SIE is based on December data. 5) The predicted PCs are
273 combined with the respective eigenvectors to produce a spatially-resolved SIC
274 anomaly prediction for each variable combination. 6) We evaluate the prediction skill
275 measured by the SIC anomaly correlation coefficient (ACC), percentage of grid points
276 with significant ACC (PGS), and root mean square error (RMSE) using cross-
277 validated model experiments to identify the superior model for each season. 7) The
278 complete SIC anomaly prediction can then be generated by combining predicted PCs
279 by the corresponding optimal model in each season with eigenvectors. We
280 differentiate the seasons as follows: winter (December through February), spring
281 (March through May), summer (June through August), and autumn (September
282 through November). 8) The predicted SIC anomalies are divided by weight value 2,
283 multiplied by standard deviation, and added the climatology to generate the complete
284 prediction field.

285 To determine model variables and the number of modes to be used in the model,
286 we evaluate the prediction skill at all grid points and all seasons in a cross-validated
287 fashion for the period 1980-2020, by calculating the ACC and RMSE between
288 predictions and observations. Notably, the dramatic declining trend in SIC prohibits
289 us to use the first half of the time series for training the model and the second half of
290 the time series to validate the model since the climate system mean state has changed
291 dramatically over the last four decades. Another cross-validation scheme (Barnston
292 and Ropelewski, 1992) is jackknifing, where one case is withheld from the regression
293 development in the Markov model as an independent sample for testing. Thus, we
294 built a Markov model for each month with a 1-yr moving window of data removal,
295 and then used this window of ~~predictions~~data to evaluate the model
296 ~~predictions~~performance. Here, we subtract one-year data from PCs and recalculate the
297 transition matrix in equation (4); then twelve-month predictions are generated for that
298 year. This procedure is repeated for each year of the time series. Such a cross-

299 validated experimental design reduces artificial skill without compromising the length
300 of the time series.

301 The long-term trend is an essential part of the Arctic sea ice variability. A
302 substantial declining trend exists in Arctic SIC, particularly in the Barents Sea, the
303 Kara Sea, the Beaufort Sea, and the Chukchi Sea (Figure 1). However, outside of the
304 Arctic Basin, the long-term trends are relatively weak in the Pacific sector. As the
305 trends are parts of the total variability, we retain the SIC trends in anomalies while
306 building the model and then conduct a post prediction evaluation of the impact of
307 trends on the model skill.



310 **Figure 1.** Arctic SIC trends (left) and standard deviation (right) computed using
311 SIC anomalies over all 12 months of the period 1979-2020. The Pacific-Arctic model
312 domain is enclosed by blue lines, which covers 40° - 84°N and 120° - 240°E. Two

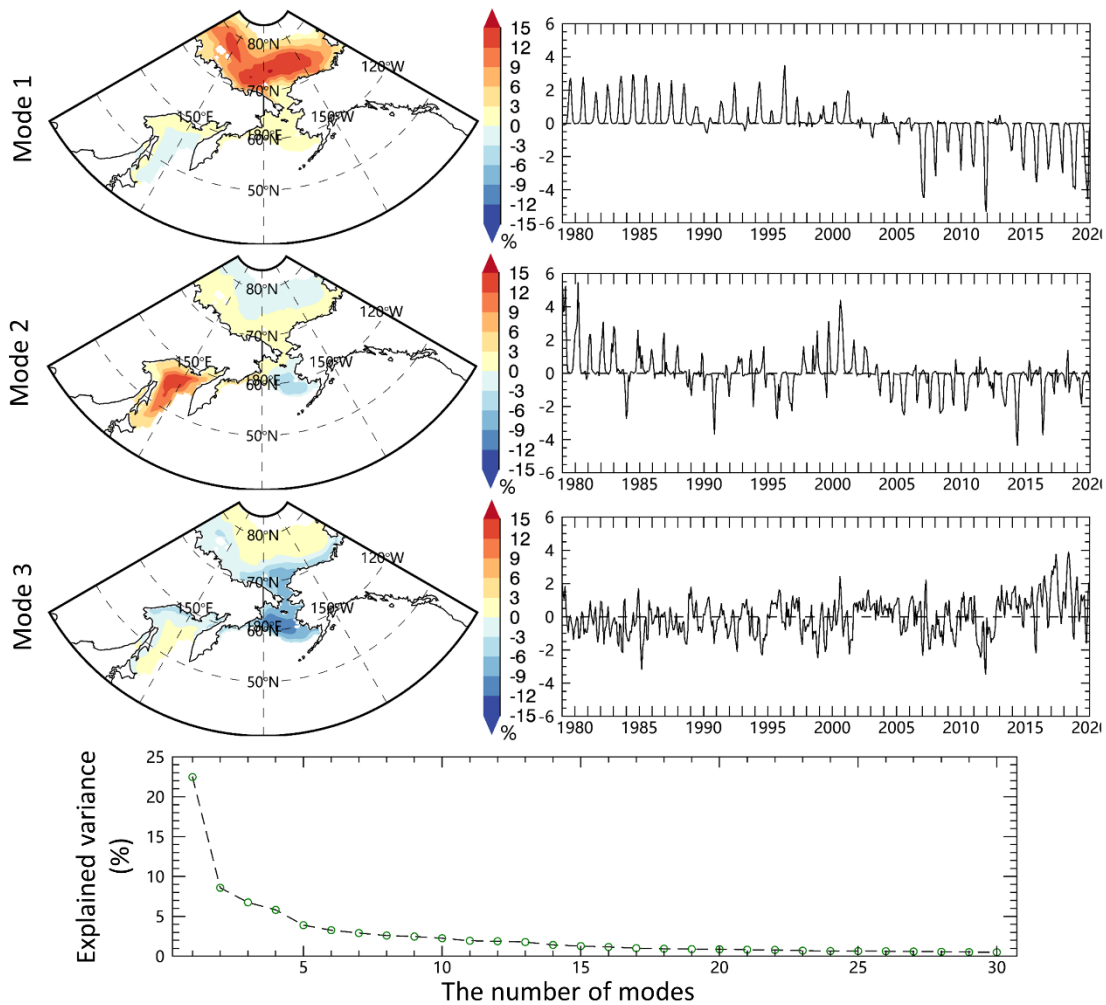
313 focused areas marked in ~~black~~ boxes in the Bering Sea (between 58°- 62°N and
314 182°-192°E) and the Sea of Okhotsk (between 52°- 56°N and 144°-152°E) have large
315 standard deviations and are selected to evaluate the ACC skill improvement in the
316 regional model compared with the pan-Arctic Markov model developed by Yuan et
317 al. (2016).

318 **3 Model construction and assessments**

319 **3.1 EOF analysis of Pacific SIC**

320 Before constructing the model, we first examine whether the EOF analysis can
321 isolate the regional and seasonal SIC variability in the Pacific–Arctic sector. Figure 2
322 shows the eigenvectors of the three leading EOF modes of SIC. The first mode of SIC
323 variability, accounting for 23% of the total variance, mainly shows a positive pattern
324 within the Arctic Basin from 1979 to 2002 and a negative pattern after 2003 with a
325 record low in 2007 and 2012, representing the decreasing trend in summer and early
326 fall SIC. The declining trend is heavily loaded inside the Arctic Basin from the East
327 Siberian Sea to the Beaufort Sea. The second SIC mode (9% of total variance)
328 primarily captures out-of-phase SIC anomalies in the Bering Sea and the Sea of
329 Okhotsk and is associated with the Aleutian-Icelandic low seesaw, representing SIC
330 variability in cold seasons (Frankignoul et al., 2014). This pattern suggests
331 consistently positive SIC anomalies in the Bering Sea and negative anomalies in the
332 Sea of Okhotsk after 2004, with a positive pattern in the Bering Sea after 2004 and an
333 opposite phase in the Sea of Okhotsk, which represents SIC variability in cold seasons
334 and is associated with the Aleutian-Icelandic low seesaw (Frankignoul et al., 2014).
335 The SIC variability in the central sector (approximately 60°-70°N) stands out in the
336 third EOF mode (7% of the total variance), which is a commonly observed feature in
337 the region during spring and autumn. This finding shows that the EOF (MEOF)
338 analysis can well isolate the regional and seasonal SIC variability including the trend
339 in the Pacific-Arctic sector.

340 We further divided the SIC time series into four seasons and conducted EOF
 341 analysis respectively. The results show that fewer modes can explain the dominant
 342 SIC variance in autumn and summer benefiting from the large SIC variability and
 343 trend (Figure S1). For example, the leading 10 modes can explain 70% of the SIC
 344 total variance in autumn and summer, while about 25 modes are needed for explaining
 345 the same amount of variance in the cold seasons. It turns out that the several leading
 346 modes can explain the dominant SIC variability. This is an important premise to
 347 reduce the model dimension and, more importantly, to filter out incoherent small-
 348 scale features that are likely unpredictable. In addition, it is necessary to build the sea
 349 ice prediction model for individual seasons because of the differences in seasonal
 350 patterns of variability and the different number of leading modes required to capture
 351 predictable this variability.



352

353 **Figure 2.** The eigenvectors and PCs of the three leading ~~three~~-EOF modes of SIC
 354 in the Pacific-Arctic~~Aretic-Pacifia~~ sector for the period 1979-2020. The bottom panel
 355 shows the explained variance as a function of the number of leading modes of SIC.

356 **3.2 Construct an optimal model for each season**

357 A practical issue in building a Markov model in MEOF spaces is which
 358 combination of variables and number of leading modes to retain in the model. Using
 359 too few modes may miss some predictable signals, and too many may result in
 360 overfitting and contaminate the model with incoherent small-scale features. To
 361 determine optimal predictor variables and reasonable mode truncations, we calculate
 362 the prediction skill from a series of cross-validated model experiments, which used
 363 different numbers of modes and different variables. Table 1 shows the detailed
 364 variable-combinations. Models V2-V4, V6-V8,⁷ and V10-V11⁹ are weighted towards
 365 surface-thermodynamic processes, whereas V9⁸ and V12¹⁰ represent integration of
 366 thermodynamic and dynamic processes.

367 **Table 1.** Variable combinations in cross-validated experiments. V1 represents the
 368 No. 1 variable-combination. ✓ represents the variable included in the corresponding
 369 combination.

	V1	V2	V3	V4	V5	V6	V7	V8	V9	V10	<u>V11</u>	<u>V12</u>
SIC	✓	✓	✓	✓	✓	✓	✓	✓	✓	✓	✓	✓
<u>OHC</u>		✓		✓	✓	✓	✓	✓	✓	✓	✓	✓
SST		✗	✓	✓	✗	✗	✗	✗	✗	✓	✓	✓
<u>SIT</u>					✓							✓
SAT			✗			✓	✗	✗	✗	✗		✓
Surface net turbulent heat flux				✗		✗		✓	✗	✗	✓	✓
Surface net radiative flux					✗		✓		✗	✓		✓
850hPa GPH, U, V								✗	✓	✗		✓

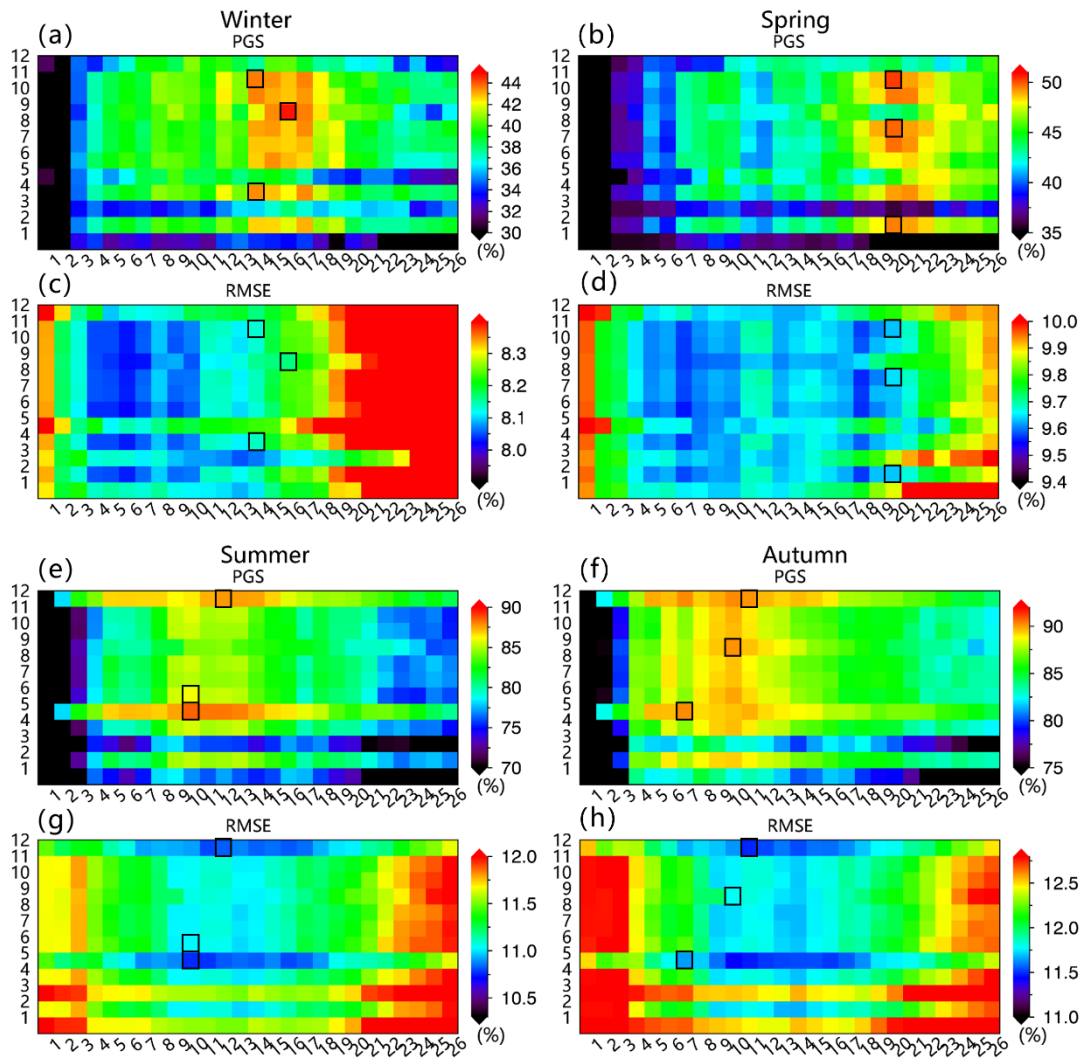
370 The cross-validation scheme is carried out for the time series to produce
 371 predictions at 1- to 12-month lead. The PGS and mean RMSE for each lead time in
 372 each season are calculated. To avoid missing predictable signals, we initially

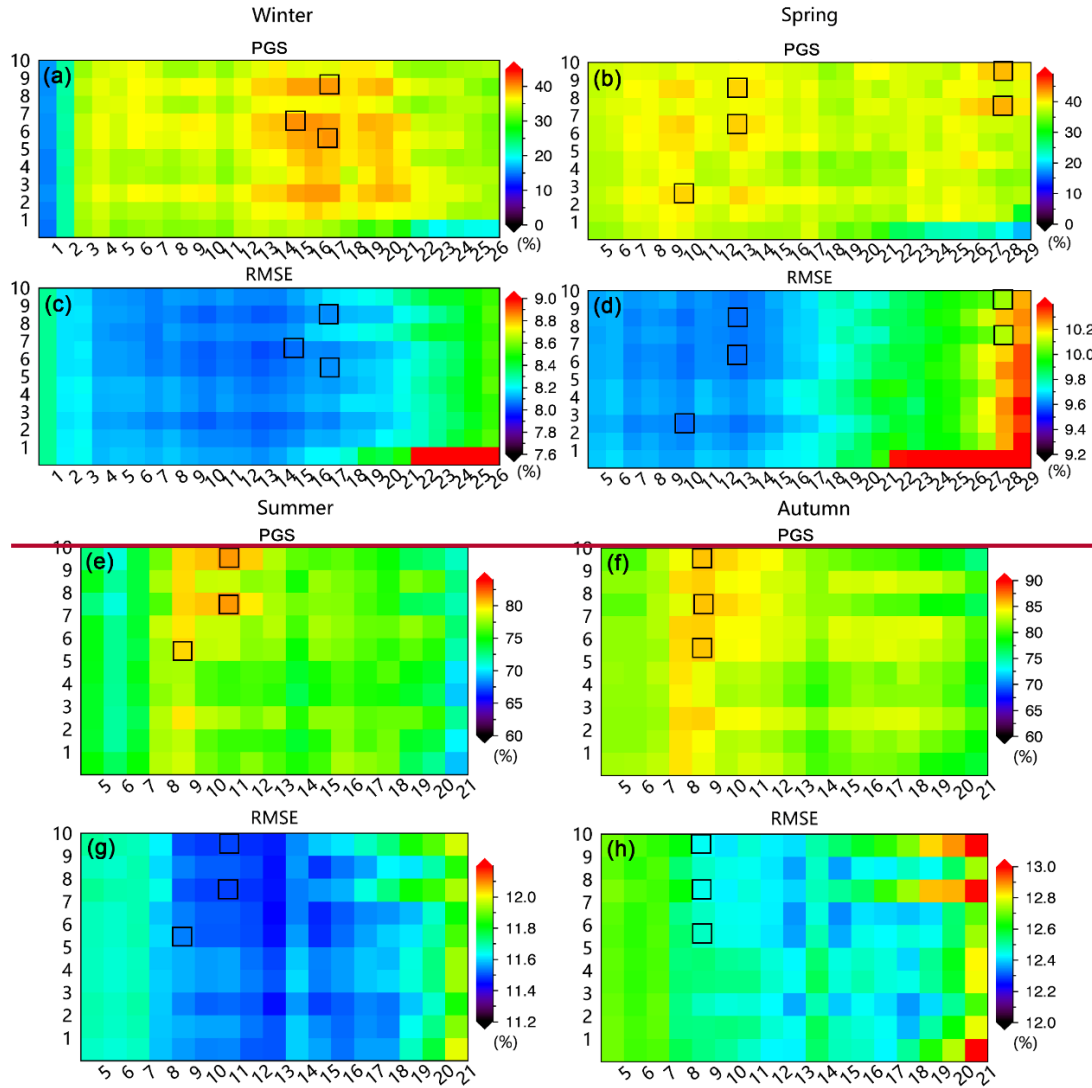
373 ~~retain~~allow large amounts of modes (up to 52) in the model and then narrow the range
374 of mode numbers to determine the best model configuration for each season. Figure
375 S2 presents the PGS for each lead time for winter target months. It shows that the
376 model prediction skill in winter steeply decreases after ~~362~~ modes in most lead
377 months. Similarly, RMSE increases rapidly after ~~362~~ modes (Figure S3). This
378 indicates that including modes beyond mode ~~362~~ in winter, mainly representative of
379 unpredictable small-scale features, leads to the rapid decrease of predictive skill.

380 To select a model configuration that fits all lead times, we average the 12 panels
381 in Figures S2 and S3, respectively, and display them in the first column of Figure S4.
382 Similarly, predictive skills for other seasons are also examined. We further
383 ~~narrow~~shrink the modes' range to display the predictive skill according to Figure S4
384 so that we can determine the optimal model more accurately (Figure 3).

385 ~~Generally~~Altogether, the model skills are better in summer and autumn than in winter
386 and spring, and more modes are needed in the cold season to capture the predictable
387 signal of SIC. ~~This indicates that sea ice in the cold season has requires more modes-~~
388 ~~to capture its variability, which is~~ likely due to the weaker trends in these months.
389 Models with high correlation also have smaller RMSE but the RMSE differences
390 between models are relatively small.

391 ~~Based on the PGS and RMSE, we primarily chose three superior model-~~
392 ~~configurations marked by black boxes in Figure 3 for winter, summer, and autumn-~~
393 ~~respectively, and chose five superior models in spring since high predictive skills are-~~
394 ~~scattered.~~





396

397 **Figure 3.** Mean PGS and mean RMSE between the observations and predictions
 398 in four seasons. (a) Mean PGS is obtained by averaging all lead months for winter
 399 predictions. The x-axis represents the number of MEOF modes, and the y-axis
 400 represents the combination of the variables corresponding to Table 1. (b, e, and f) are
 401 the same as (a) except for spring, summer, and autumn respectively. (c, d, g, and h)
 402 are the same as (a, b, e, and f) except for RMSE.

403 Based on the PGS and RMSE, we primarily chose three superior model
 404 configurations marked by black boxes in Figure 3 for each season respectively. To
 405 determine which model configuration produces the best prediction in each season, we
 406 spatially average the SIC prediction skill from these superior models with 1- to 12-
 407 month leads (Figures 4 and 5). Figure 4 shows the cross-validation skill measured by

408 PGS. In general, the predictive skill in ~~summer and autumn~~the warm season is higher
409 ~~(by roughly 35%)~~ than that in ~~winter and spring~~the cold season, although the RMSEs
410 are also relatively large in the warm season (Figure 5). The model prediction skills
411 based on those superior model configurations have similar variability and magnitude
412 in winter and spring respectively, while large differences of that occur in the warm
413 season, especially in autumn. It also shows that the model prediction skill steeply
414 decreases at the 2-month lead in winter and at the 2- and 3-month lead in spring.
415 ~~These models also exhibit a local minimum of PGS in each season at a 10-month lead~~
416 ~~for winter, at a 3-month lead for spring, at a 4- and 6-month lead for summer, and at a~~
417 ~~7-month lead for autumn. In other words, the seasonal models show a common-~~
418 ~~feature of low prediction skill for forecasts initialized in the month of March, but~~
419 ~~show higher skill at lead times beyond this, suggesting that certain sources of~~
420 ~~predictability present in March are absent in these models.~~

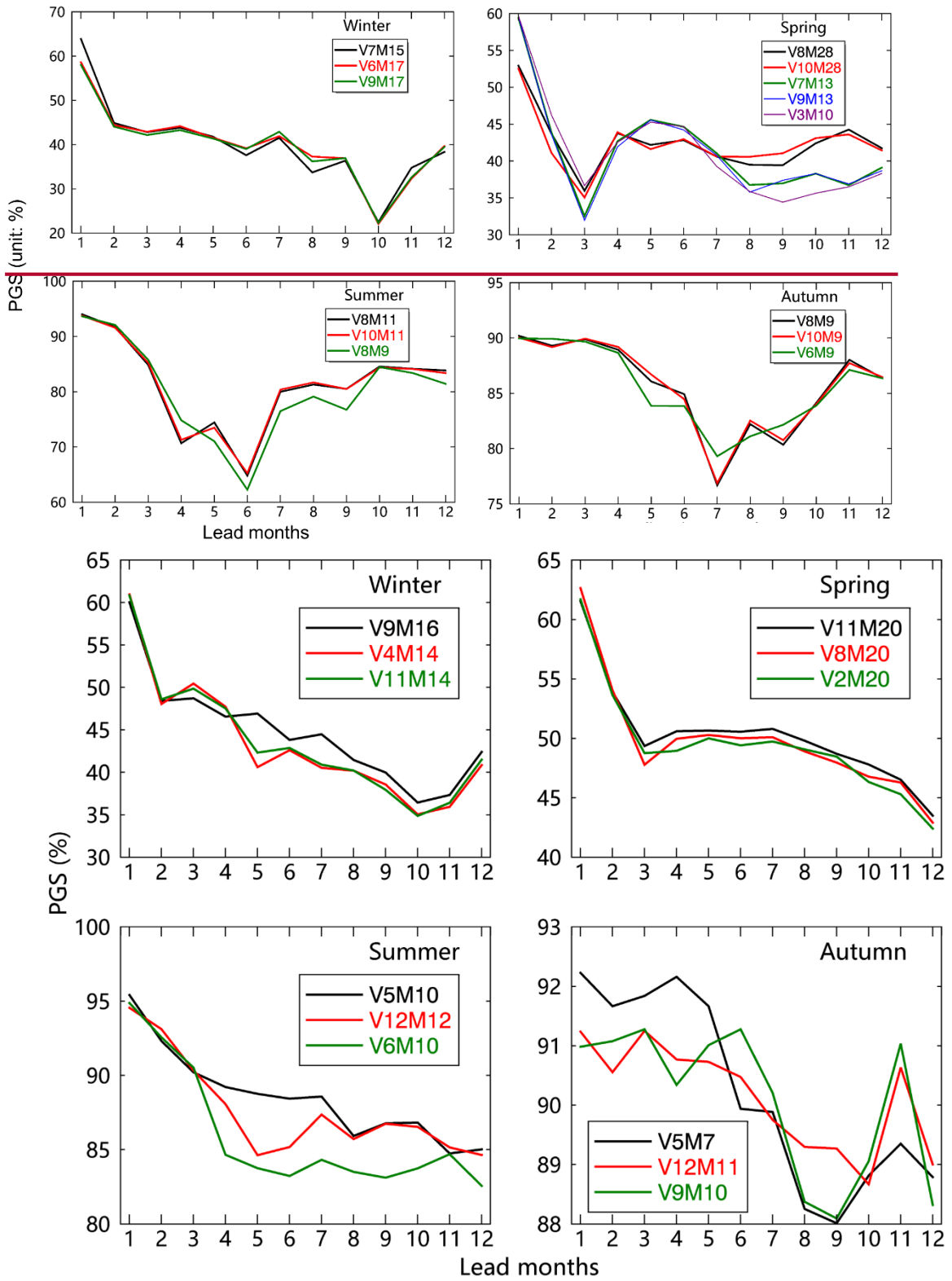
421 As a model construction principle, we choose the minimum number of variables
422 and modes to achieve the same level of skill, avoiding possible overfitting. Based on
423 the PGS and RMSE, we chose ~~V9M16~~V7M16 as the best model as the best model in
424 winter since it shows the ~~lowest~~highest RMSE/PGS. Similarly, we chose ~~V11M20~~ in
425 ~~spring and V5M10~~ in summer. In autumn, The model skill from ~~V5~~ is obviously
426 ~~superior at 1-5 lead months, while V12 dominates prediction skill beyond the 8-month~~
427 ~~lead. We decided to choose V5M7 because it has a relatively higher mean skill and~~
428 ~~fewer variables and modes. In spring, we ruled out V8M28 and V10M28 because of~~
429 ~~the large RMSE and chose V7M13 since it shows a slightly larger correlation among~~
430 ~~the rest of the models. In the warm season, V8 and V10 show nearly the same skill,~~
431 ~~indicating that the surface turbulent heat flux and radiative flux do not contribute to~~
432 ~~the model skill. So we selected the V8M11 in summer and V8M9 in autumn.~~

433 The contribution of different variables in ice prediction skill for each season is
434 also assessed. OHC contributes more model prediction skill than SST in all seasons
435 (Figure 3). The model built on the data matrix of SIC, OHC performs better in winter
436 and spring, which indicates that the OHC provides a considerable source of memory

437 for SIC prediction skill in the cold season and plays a key role in the evolution of sea
438 ice conditions. The results are consistent with many previous studies (Bushuk et al.,
439 2017a; Dai et al., 2020; Guemas et al., 2016b; Lenetsky et al., 2021). 850 hPa
440 geopotential height and winds can still contribute additional prediction skill in winter
441 since including OHC, geopotential height and winds slightly outperforms the case
442 without geopotential height and winds (Figure 4). 850 hPa GPH and wind not only
443 affect the heat and moisture transport by atmospheric circulation anomaly but also
444 drive sea-ice drift. For example, the dipole structure anomaly of the Arctic
445 atmospheric circulation shows strong meridionality and plays a profound role in sea-
446 ice export/import, and heat and moisture transport through the Pacific-Arctic sector
447 (Wu et al., 2006).

448 Similarly, SST and turbulent heat flux also contribute additional skill in spring
449 although the contribution is minor (Figures 3 and 4). It is worth mentioning that the
450 variable such as SST with minor additional contributions to the model does not mean
451 that it is a minor contributor since the contributions from different variables to
452 prediction skill partially overlap. In addition, adding SIT to the model has a
453 substantial contribution to the prediction skill in the warm season, indicating that sea
454 ice thickness is a key source of sea ice predictability within the Arctic Basin in the
455 warm season especially in summer, which is consistent with previous studies
456 (Blanchard-Wrigglesworth et al., 2011; Blockley and Peterson, 2018; Day et al.,
457 2014a; Morioka et al., 2021; Tian et al., 2021; Yuan et al., 2016). However, SIT has a
458 negative contribution to the prediction skill in the cold season (Figure 3). The
459 contributions of SIT to the prediction skill in autumn are very sensitive to the number
460 of lead months that the skill steeply decreases beyond a 5-month lead (Figure 4). In
461 other words, the model didn't perform well in autumn prediction initialized in winter
462 and spring. In addition ~~to SIC, SST, and SAT,~~ the surface net radiative flux mainly
463 also contributes to the model skill in the cold season (Figure 3), reflecting Early
464 studies suggested that the surface longwave radiation plays an
465 indispensable significant role in the polar climate system in the cold season when

466 shortwave radiation is at its annual minimum. ~~Previous studies suggested that cloud~~
467 ~~cover is capable of controlling sea ice growth processes through its influences on the~~
468 ~~surface energy budget via transmitting longwave radiation~~ (Huang et al., 2015;
469 Kapsch et al., 2013; Lee et al., 2017; Liu and Key, 2014; Luo et al., 2017; Wang et
470 al., 2019b). ~~On the other hand, argued that negative cloud anomalies combined with~~
471 ~~increased surface solar radiation in summer had no substantial contribution to the~~
472 ~~minimum SIE record in 2007. conclude that the accumulation of surface downwelling~~
473 ~~shortwave radiation did not correspond well to negative SIC anomalies in summer.~~
474 ~~Our model experiments also suggest that the surface net radiative flux does not~~
475 ~~contribute to the prediction skill in warm season. Instead, 850 hPa GPH and wind, not~~
476 ~~only affect the heat and moisture transport by atmospheric circulation anomaly but~~
477 ~~also drive sea ice drift, mainly contribute to the model skill in warm season. For~~
478 ~~example, the dipole structure anomaly of the Arctic atmospheric circulation shows~~
479 ~~strong meridionality and plays a profound role in sea ice export/import, and heat and~~
480 ~~moisture transport through the Pacific Arctic sector~~ (Wu et al., 2006).

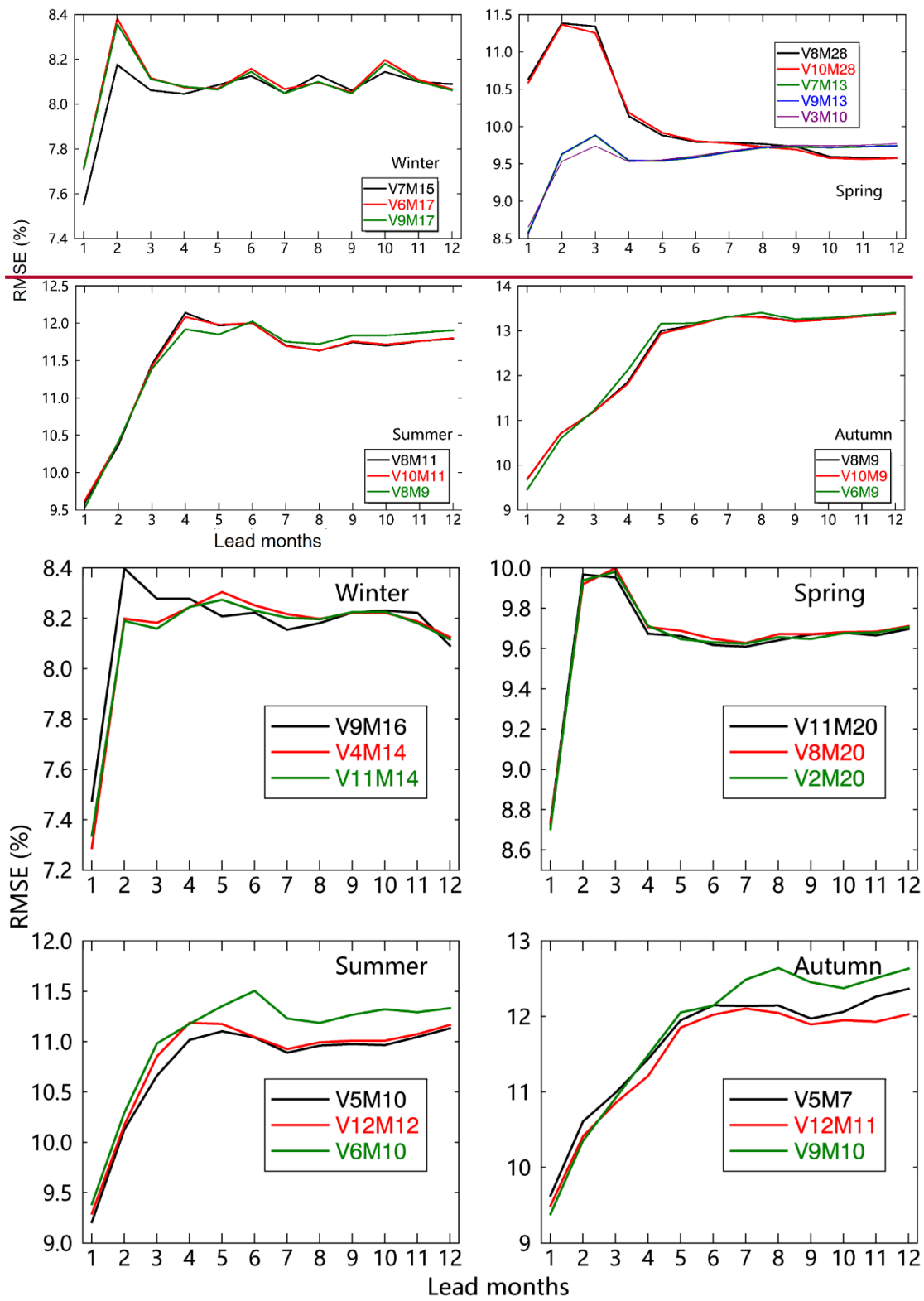


481

482

483

Figure 4. PGS for the preliminary selection of superior models in each season.



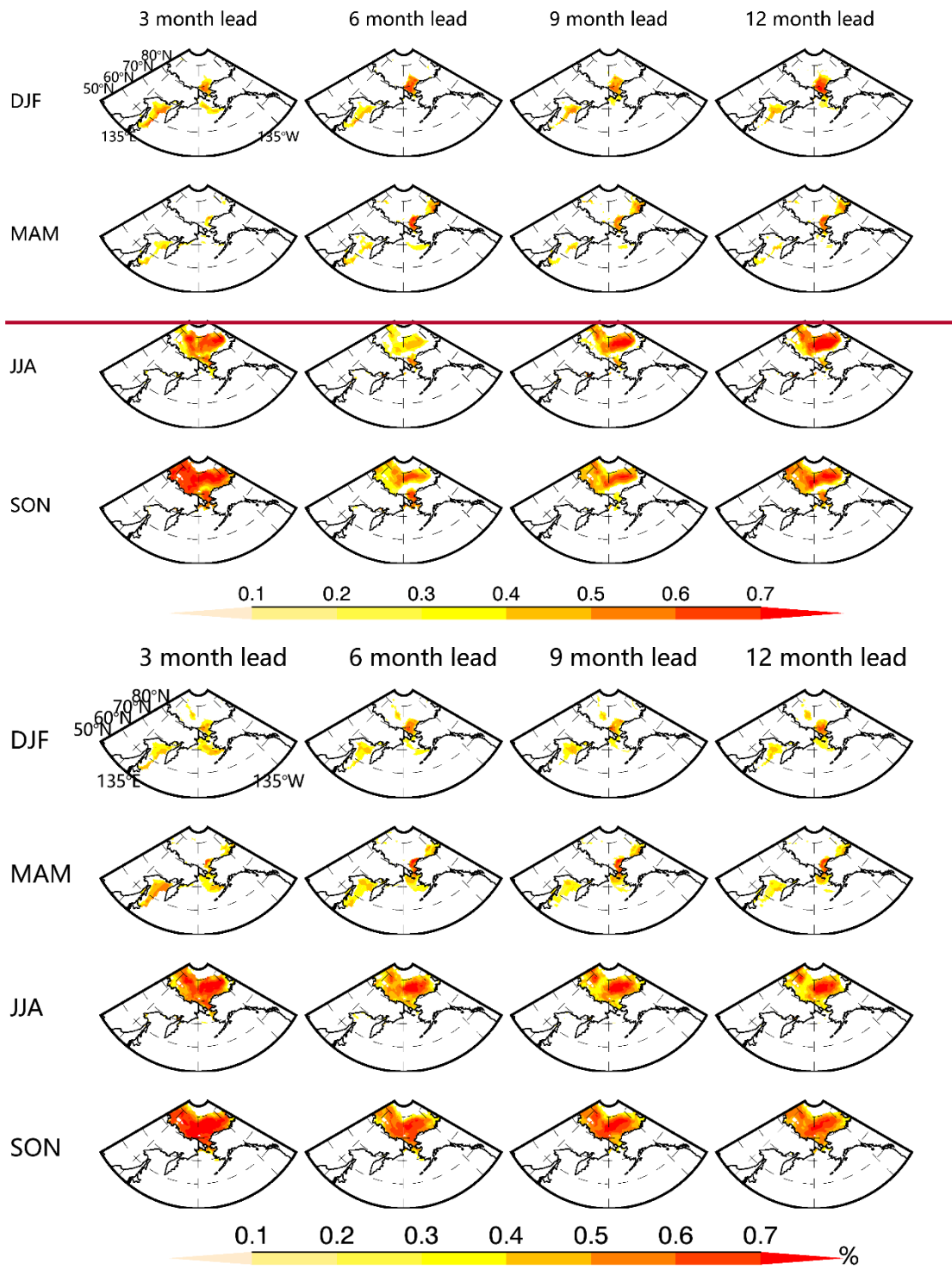
484

485

486 **Figure 5.** Same as Figure 4 but for RMSE.

487 **3.3 Assessment of model skill**

488 To test the forecast skill of the model, the SIC predictions were evaluated at each
489 grid cell and for all seasons using the ACC and RMSE between predicted and
490 observed anomalies, and the skill is presented at 3, 6, 9, and 12 lead months. In winter
491 (DJF), high forecast skill is concentrated in the Arctic marginal seas and peripheral
492 seas: the ~~northern~~southern Chukchi Sea~~Bering Strait~~ and ~~northern~~-Sea of Okhotsk
493 (Figure 6). The skill is slightly lower at a ~~12~~-month lead in the Sea of Okhotsk and
494 ~~from a 6-month to a~~ 9-month lead in the southern Chukchi Sea~~Bering Sea~~, whereas
495 ~~high skill values (>0.6) are maintained up to a 12-month lead in the Bering Strait.~~
496 Overall, the winter skill is roughly 0.4 in the Sea of Okhotsk and 0.5 in the southern
497 Chukchi Sea at up to 12-month leads. The spring (MAM) prediction skill shows a
498 similar pattern as that in winter but with a 0.1 ~~increase~~reduction in the ACC skill. The
499 southern Chukchi Sea and Bering Strait have higher skills than the Bering
500 Sea~~southern part of the strait~~. For summer (JJA) predictions, the prediction skill is
501 concentrated in the Arctic basin since sea ice ~~nearly~~-totally melts in the Arctic
502 peripheral seas. The 3-month lead prediction has the highest skill (>0.6) in most of the
503 Arctic basin, while the lowest prediction skill (<0.54) is found at a ~~12~~-month lead.-
504 ~~This skill dip indicates that using winter SIC to forecast summer sea ice is~~
505 ~~unsatisfactory. However, the 9-month and 12-month lead predictions again show high~~
506 ~~skill (>0.6) in most of the Arctic Basin.~~The autumn (SON) prediction skill shows a
507 similar pattern as the summer skill but with higher correlations ~~than that in summer~~.
508 ~~For targeted autumn predictions, the significantly increased skill at 6-month lead~~
509 ~~relative to other seasons could be related to the sea ice anomaly reemergence from~~
510 ~~spring to autumn due to the oceanic memory~~ (Blanchard-Wrigglesworth et al., 2011)-
511 ~~Still, the autumn prediction skill at a 6-month lead is lower than that at other lead~~
512 ~~months, indicating that the impact of the spring predictability barrier on prediction~~
513 ~~was not offset by the SST anomaly reemergence.~~In general, the model has higher
514 prediction skills for warm seasons, especially for autumn, than that for cold seasons,
515 while the lowest skill is in spring~~winter~~.

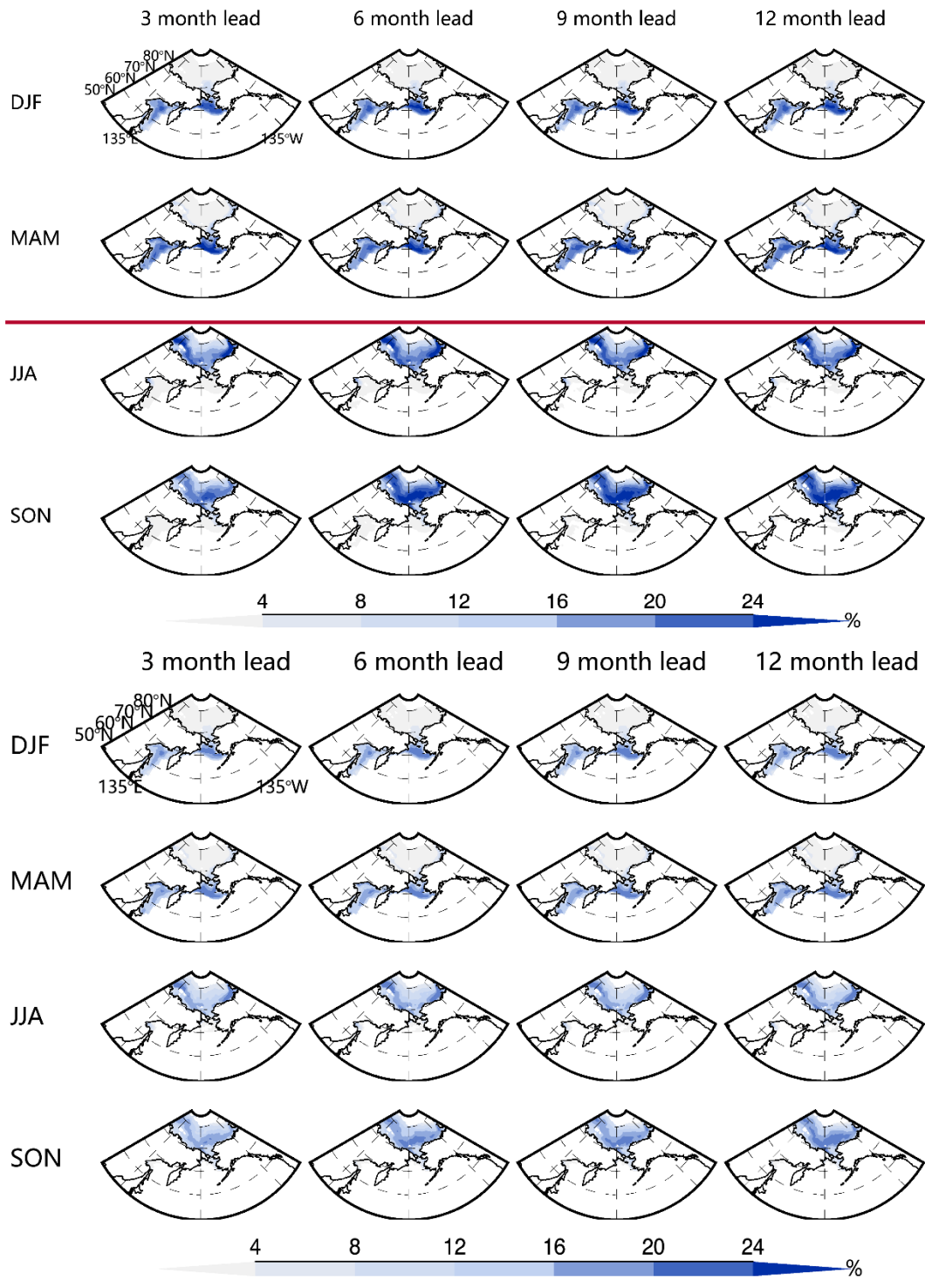


516

517

518 **Figure 6.** Cross-validated model skills measured by ACC between SIC
 519 predictions and observation anomalies as a function of seasons and lead months. Only
 520 the correlations that are significantly above the 95% confidence level based on a
 521 Student's t test are included in the panels.

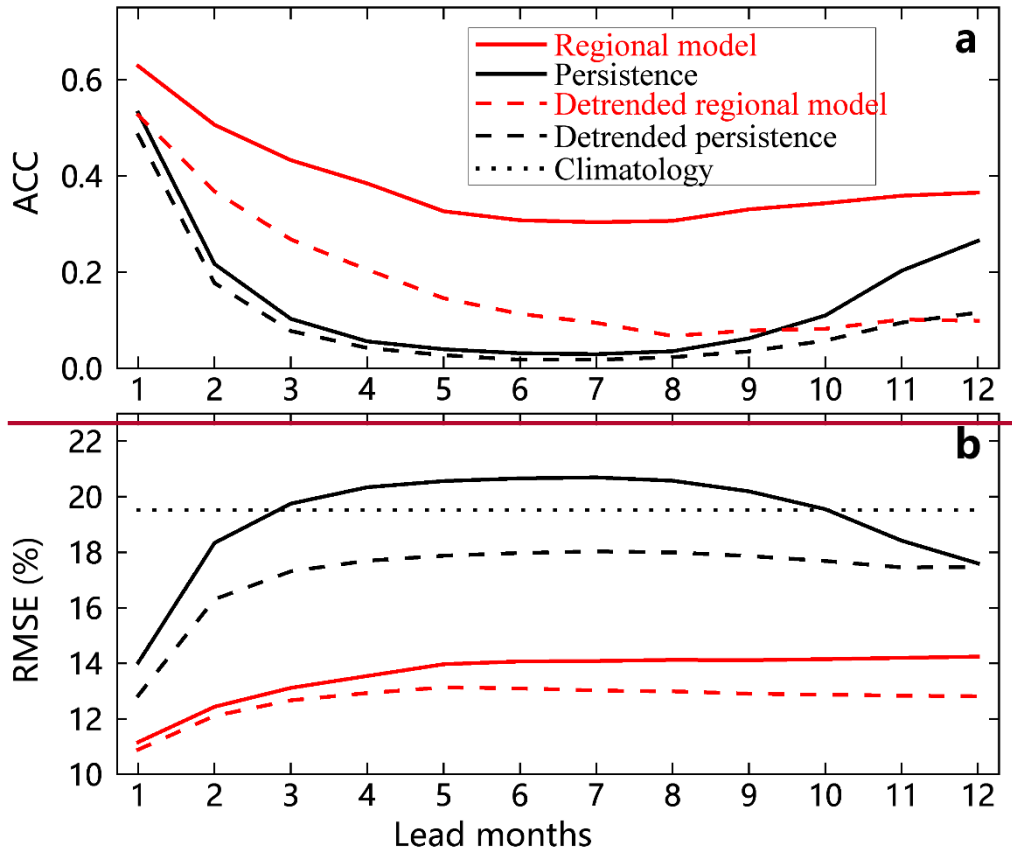
522 RMSEs are consistent with correlations: high correlations correspond to low
523 RMSEs, and vice versa, although minor inconsistencies occur in some seasons and
524 regions (Figure 7). The RMSE is large around the Arctic basin for the warm season
525 and in the peripheral sea for the cold season where SIC has large variability. In the
526 cold season, the RMSE is larger in the Bering Sea than that in the Sea of Okhotsk.
527 The magnitudes of RMSE remain at roughly the same level from 3- to 12-month lead
528 ~~and all seasons~~ in most locations for all seasons. The marginal seas have larger
529 RMSEs than the central Arctic basin in both summer and autumn, while the error
530 magnitudes in autumn are slightly larger than those in summer but smaller than the
531 SIC standard deviation across the Pacific sector (Figure 1).



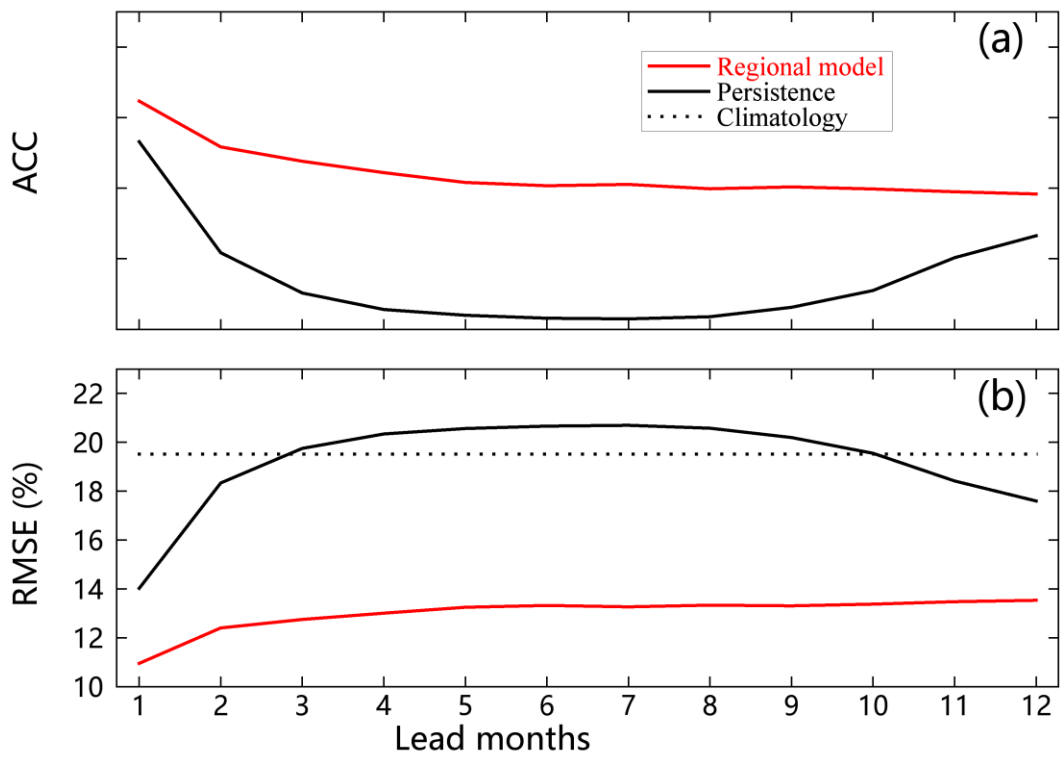
534 **Figure 7.** Same as Figure 6 except for RMSEs. The color bar is in a unit of
 535 percentage%.

536 Also, the model performance is further evaluated against anomaly persistence and
 537 climatology. Averaged over the grid points in the model domain and over all seasons
 538 for the period of 1980-2020, the regional Markov model's mean correlation is

539 manifestly higher, and the mean RMSE of the regional Markov model is much lower
540 ~~than still quite skillful compared with~~ the climatology and anomaly persistence for all
541 the lead months ~~whether the sea ice trend is removed or not~~, especially from 2-month
542 lead to 10-month lead (Figure 8). In addition, RMSE is not sensitive to the lead
543 months, showing the superiority of the regional model. These results suggest that the
544 regional Markov model can capture significantly more predictability beyond SIC
545 anomaly persistence. ~~This indicates that there are crucial sources of predictability~~
546 ~~beyond SIC anomaly persistence that the regional Markov model is able to capture.~~



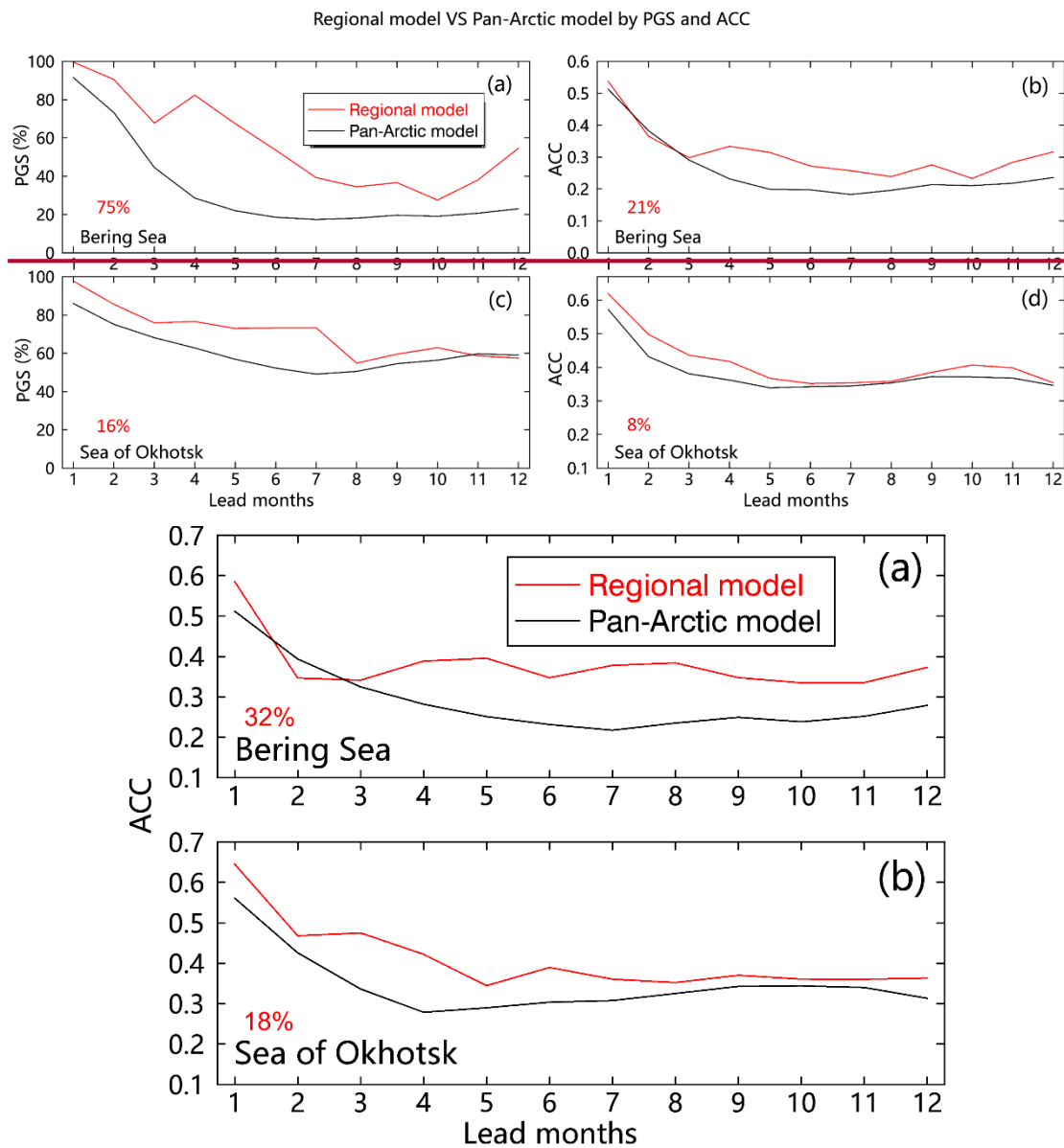
547



548

549 **Figure 8.** The prediction skill of the regional Markov model compared against
550 that of anomaly persistence and climatology averaged over the model domain as a
551 function of the number of month lead times.

552 To assess the regional model skill improvements from the pan-Arctic model
553 presented by Yuan et al. (2016), we calculated the ~~PGS and~~ ACC as a function of lead
554 months (Figure 9). Note that ~~the PGS is calculated in the entire area for the Bering-~~
555 ~~Sea and the Sea of Okhotsk, and~~ the ACC is calculated only in typical regions with
556 large standard deviations marked in Figure 1. The regional model evidently
557 ~~substantially~~ enhances the ~~PGS-ACC~~ skill from the pan-Arctic model for the ~~42-~~ to
558 12-month lead predictions in the Bering Sea and the 1- to 7-month lead predictions in
559 the Sea of Okhotsk. The ~~mean PGS improvement is 75% in the Bering Sea and 16%~~
560 ~~in the Sea of Okhotsk. Similarly, the~~ ACC is also increased by ~~3221%~~ in the Bering
561 Sea and ~~188%~~ in the Sea of Okhotsk. The prediction skill of the regional Markov
562 model ~~within~~ the Arctic basin also remains at the same high level as that of the Pan-
563 Arctic model (not shown), so significant skill improvements occur in the peripheral
564 sea of the Pacific sector, ~~demonstrating the superiority of the regional model.~~



565

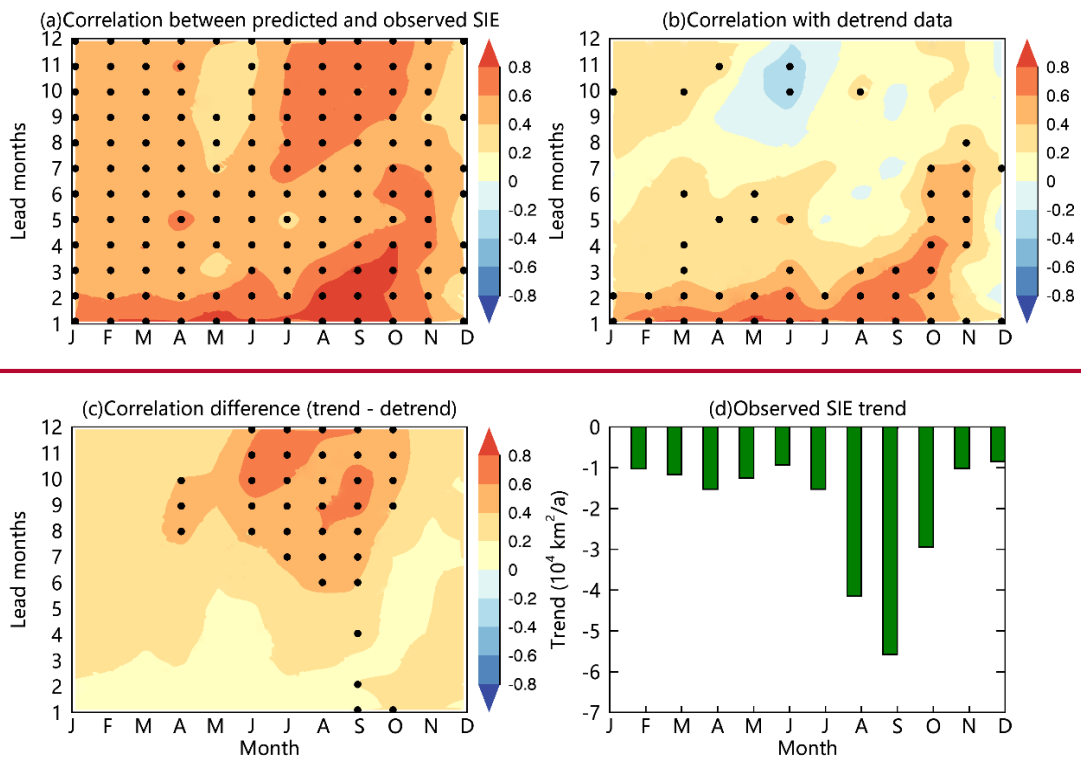
566

567 **Figure 9.** Cross-validated model skills of the regional Markov model vs. the Pan-
 568 Arctic Markov model. (a-e) The skills are measured by the PGS-ACC between
 569 predictions and observations with trends from 1980 to 2020 as a function of lead
 570 months in the Bering Sea ~~and the Sea of Okhotsk~~. (b, d) ~~are is~~ the same as (a, e)
 571 except for the Sea of Okhotsk ~~the ACC~~. The red numbers in the bottom left ~~bottom~~ of
 572 each panel represent the mean regional model skill improvements from the pan-Arctic
 573 model.

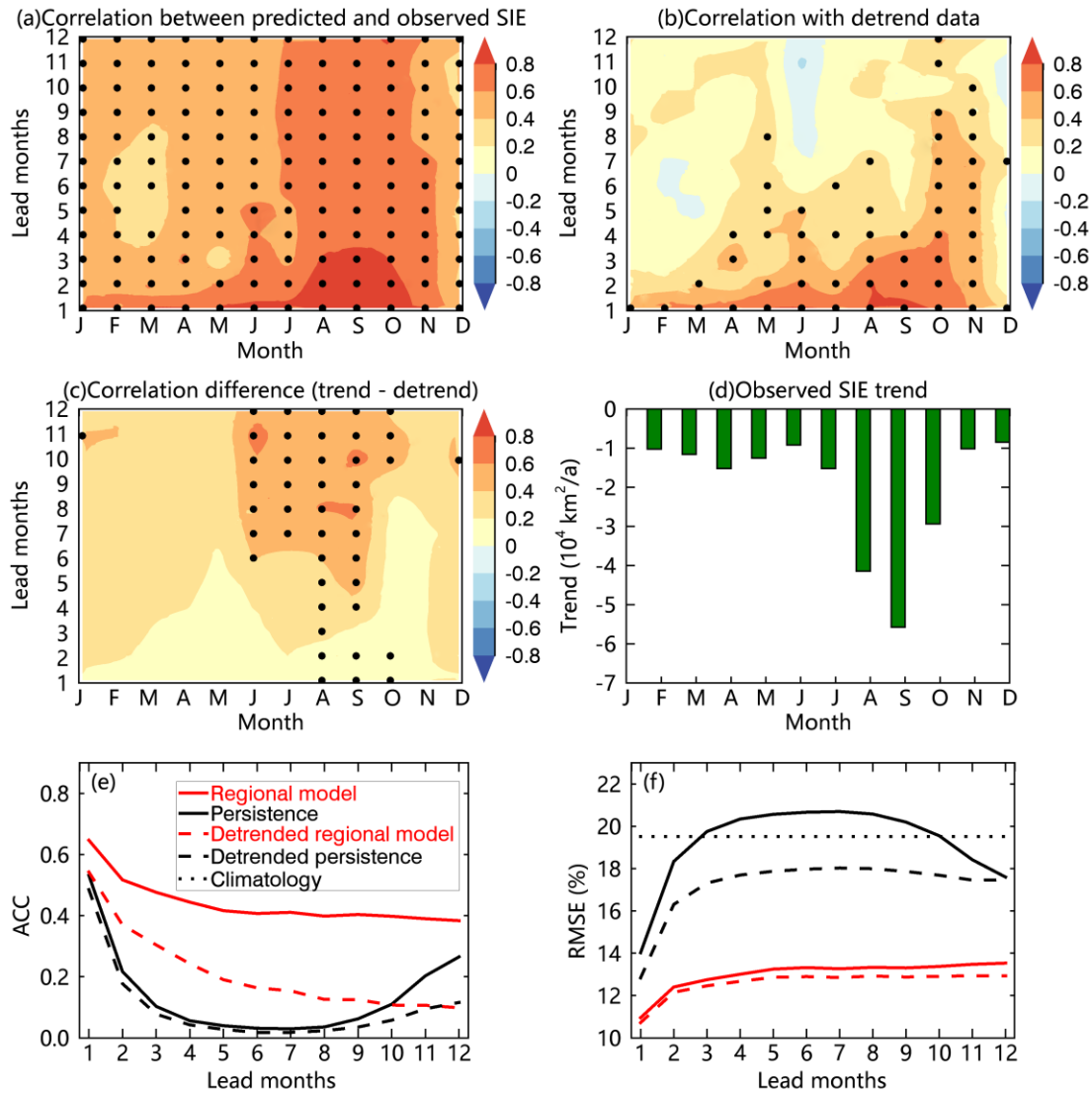
574 **4 Discussion**

575 **4.13.4 Contribution of linear trends to SIE prediction skill**

576 Sigmoid et al. (2013) show that the linear trend in Arctic SIE dramatically
577 contributes to its forecast skill in the Canadian Seasonal to Interannual Prediction
578 System. Lindsay et al. (2008) show that their dynamic model prediction skill is much
579 lower when the trend is not included. They suggested that the trend accounts for 76%
580 of the variance of the pan-Arctic ice extent in September. The trend also contributes
581 to the pan-Arctic prediction in the linear Markov model (Yuan et al., 2016). In the
582 Arctic, SIE has declined at -0.35 million square kilometers per decade during 1979-
583 2020, which is significant at the 95% confidence level. The large SIC trend is mainly
584 in the Barents Sea and the Kara Sea, followed by the Chukchi Sea, while the mean
585 SIC trend in the Bering Sea and the Sea of Okhotsk is relatively weak (Figure 1). To
586 evaluate the contribution of long-term trends to the regional Markov model skill, we
587 conducted post-prediction analysis on linear trends' contribution to the predictions
588 skill of SIE in the Pacific-Arctic sector. ¶ We examine the time series of SIE in all
589 calendar and lead months calculated by summing the Pacific-Arctic areas that have at
590 least 15% SIC from observations and predictions. Monthly trends were removed from
591 the predictions and observations, respectively. Then, the model skill is compared
592 between the original SIE predictions and detrended SIE predictions.



593



594

595 **Figure 10.** (a) The SIE forecast skill of the regional Markov model as a function
 596 of the calendar month and lead months. (b) The SIE forecast skill when monthly
 597 trends are removed from the predictions and observations respectively. The black dots
 598 in (a) and (b) represent the correlations that are significantly above the 95%
 599 confidence level. (c) Difference between (a) and (b). The black dots in (c) indicate
 600 that the correlation differences are significant above the 95% confidence level. (d)
 601 Observed trends in SIE as a function of the calendar month. All monthly SIE trends
 602 are significantly above the 95% confidence level. (e, f) The prediction skill of the
 603 regional Markov model compared against that of anomaly persistence and
 604 climatology averaged over the model domain as a function of the number of month
 605 lead times.

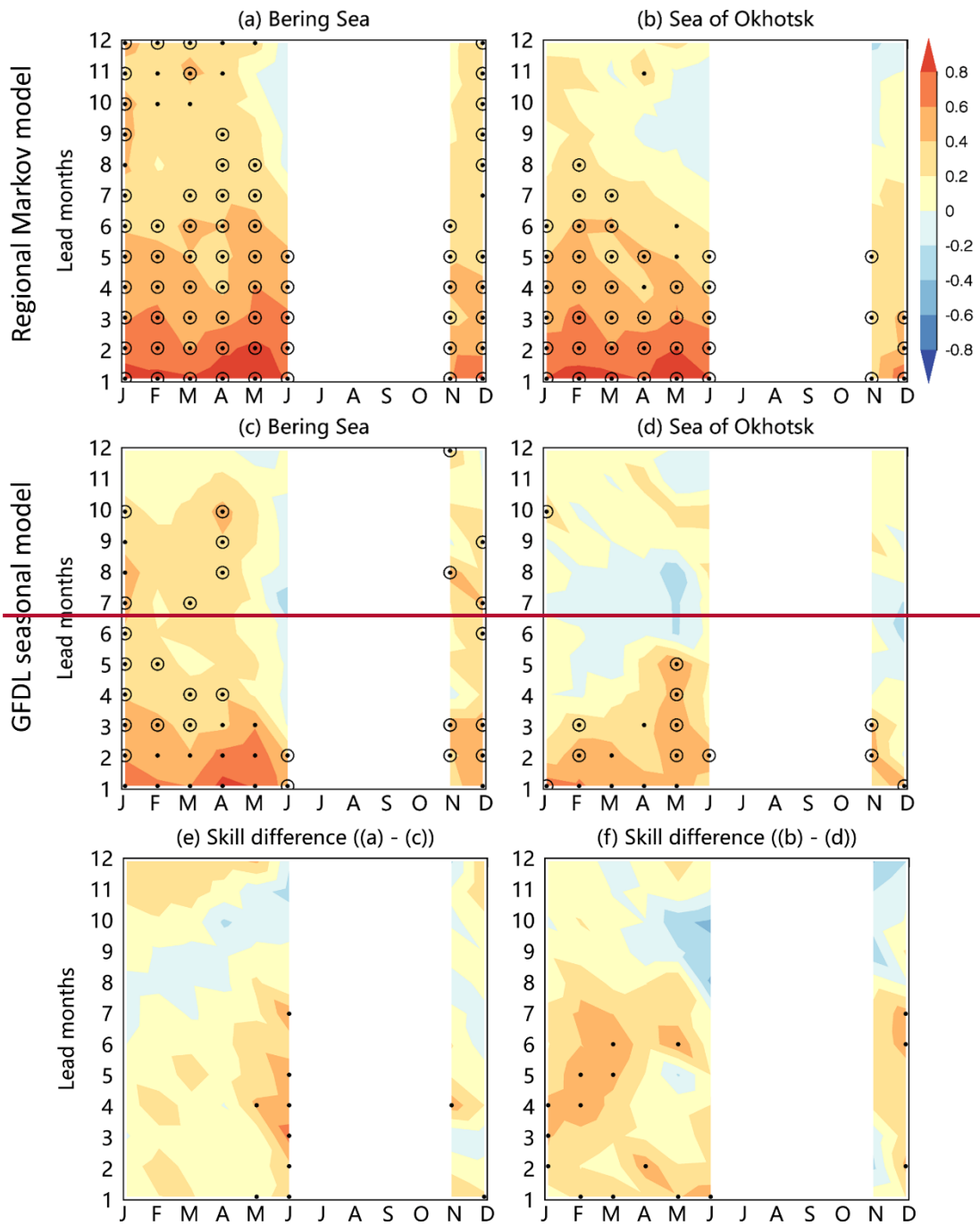
606 ~~Figure 10 shows the model skill of the SIE forecast in the Arctic Pacific sector~~
607 ~~and the contribution of linear trends to the skill.~~ The model ~~has good~~is skillful in
608 predicting SIE from January to November at a 1-~~to 2~~ month lead (Figure 10a). The
609 skill is particularly high for ~~the predictions in~~ summer and autumn predictions, where
610 ACC. It is higher than 0.6 from July through ~~October~~ November even at a 12-month
611 ~~lead months 9-12~~. The model skill is relatively low in May ~~and December~~, especially
612 at ~~84-118~~ lead months. This pattern is consistent with the seasonal variation of the
613 model skill for SIC prediction presented in Figure 6.

614 After monthly trends are removed from ~~both~~ predictions and observations_
615 respectively, the model skill is significantly reduced for all seasons, especially for the
616 warm season at 6-12 months lead (Figure 10b, c). This is consistent with the
617 seasonality of the observed trend (Figure 10d), which also peaks in late summer and
618 early fall.

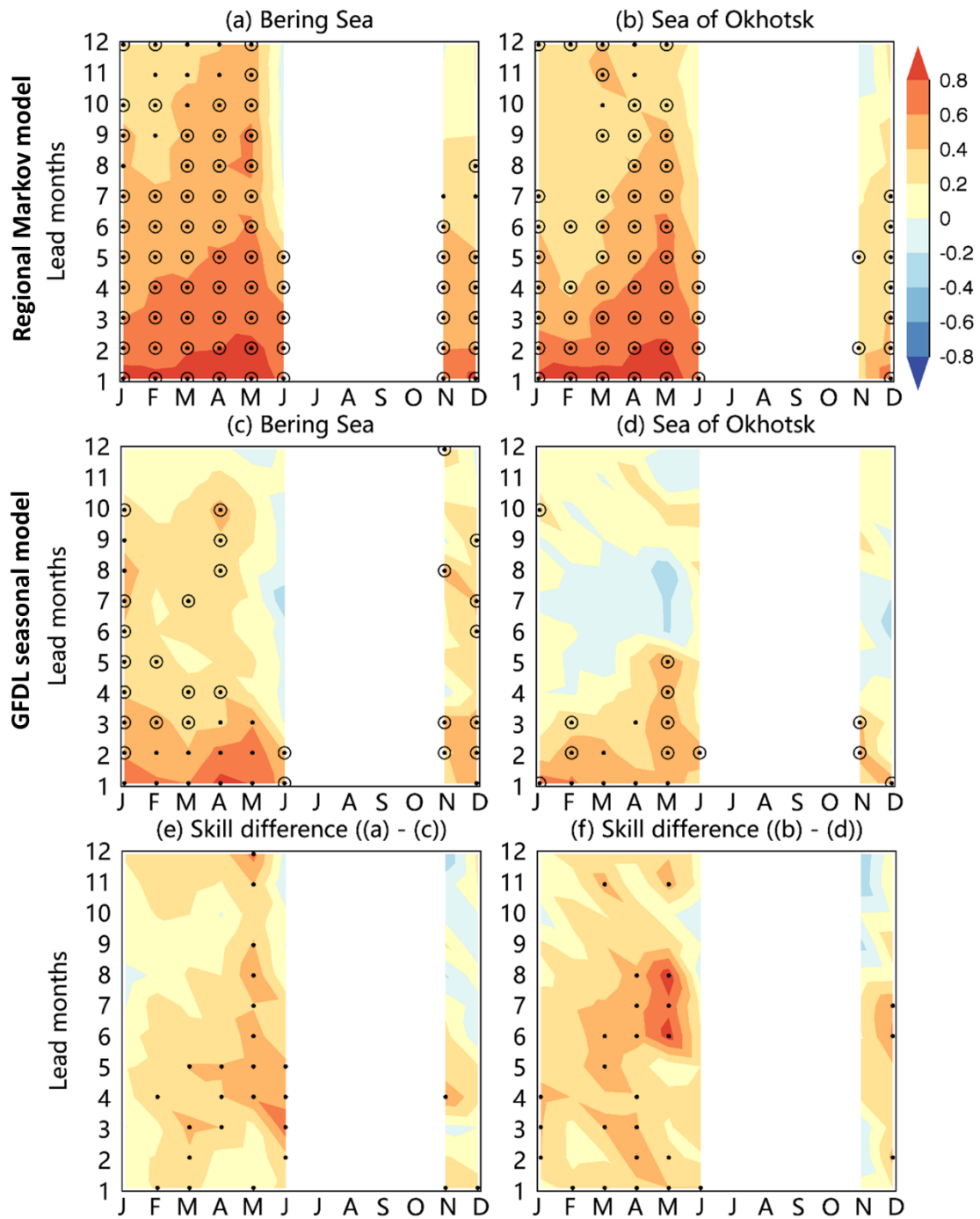
619 Averaging the differences in Figure 10c over all lead times and predicted months,
620 the trend removal results in a mean reduction of 0.31 from the SIE forecast skill; a
621 ~~535~~53% reduction of the mean ACC. However, the model retains high prediction skill
622 (0.613) from January to ~~October~~ November at 1-2 lead months, representing a ~~196~~19%
623 reduction by the trend removal ~~in these leads~~ (Figure 10b), which shows the model's
624 capability of capturing sea ice internal variability. In addition, the trend is relatively
625 large in the Chukchi Sea and weak outside of the Arctic Ocean. The model only
626 reduces ~~134~~13% of the mean ACC from January to ~~November~~ October at 1-2 lead
627 months after the trend removal for the area outside of the Arctic Ocean. Although
628 linear trends contribute significantly to the model skill, the regional Markov model's
629 mean correlation is manifestly higher, and the mean RMSE of the regional Markov
630 model is much lower than the climatology and anomaly persistence for all the lead
631 months when the sea ice trend is removed (Figure 10e, f).

632 4.23.5 Comparison with the GFDL model

633 Yuan et al. (2016) showed that the pan-Arctic Markov model consistently
634 outperforms the NOAA/NCEP Climate Forecast System (CFSv2) and the Canadian
635 seasonal and interannual prediction system for sea ice seasonal predictions. Here the
636 regional Markov model is compared with the Geophysical Fluid Dynamics
637 Laboratory Forecast-oriented Low Ocean Resolution (GFDL-FLOR) seasonal
638 prediction system (Bushuk et al., 2017a) in detrended SIE forecasts. The hindcast
639 model skills measured by the ACC for detrended SIE are high from both the regional
640 Markov model and GFDL ~~seasonal prediction system~~ model during January to June at
641 a 1- to 3-month lead in the Pacific sector (Figure 11). The regional Markov model
642 skill is statistically significant at lead times ranging from 1 to ~~65~~ months for target
643 months of January-June in both the Bering Sea and the Sea of Okhotsk. Below we
644 highlight some key differences between these two models in the Bering Sea and the
645 Sea of Okhotsk.



646



647

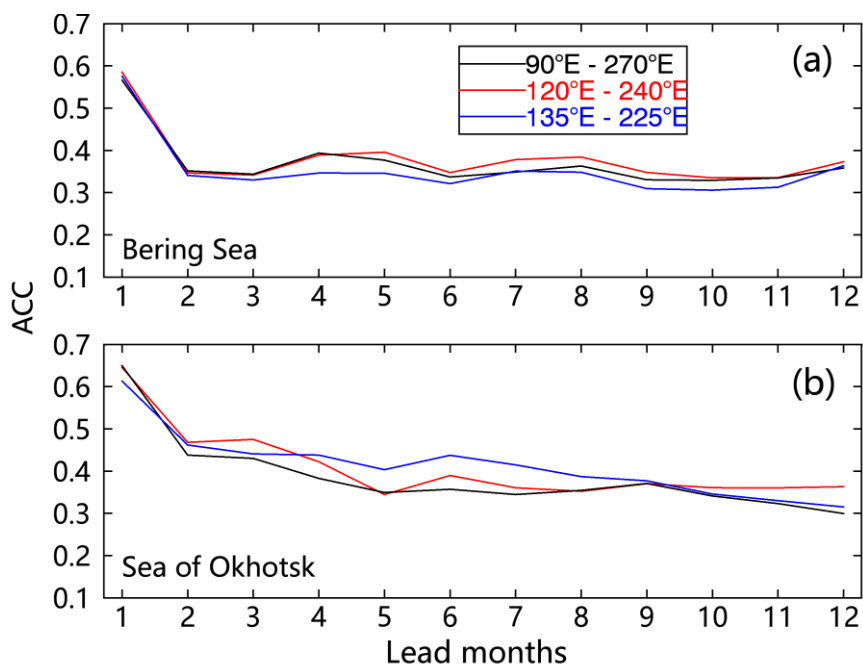
648 **Figure 11.** (a, b) Hindcast model skill (ACC) for detrended regional SIE forecasts
 649 from 1982 to 2020 for the regional Markov model. (c, d) Same as (a, b) except for the
 650 GFDL seasonal prediction system. (e, f) is the skill difference between these two
 651 models. The black dots in (a-d) represent ACCs that are significantly above the 95%
 652 confidence level, and the circles in (a-d) indicate months in which the model's skill
 653 exceeds that of a persistence forecast. The black dots in (e-f) represent ACC
 654 differences that are significant above the 95% confidence level.

655 Notably, the skill from the regional Markov model is higher than that from the
656 GFDL seasonal prediction system during February to June at 31- to 67-month leads
657 in the Bering Sea and during December to March-June at 1- to 87-month leads in the
658 Sea of Okhotsk. In the other words, the regional Markov model performs better in
659 spring prediction using winter observations for the Bering Sea and autumn
660 observations for the Sea of Okhotsk. Nevertheless, the regional Markov model
661 slightly underperforms the GFDL seasonal prediction system in predictions during
662 November to December using the previous winter and spring observations for the
663 Bering Sea and using the previous winter observations for the Sea of Okhotsk. the-
664 regional Markov model performs better in June prediction using the observations in-
665 the previous winter and spring in the Bering Sea. The model also performs better in-
666 winter to early spring prediction using the observations in previous summer and fall in
667 the Sea of Okhotsk. Nevertheless, the regional Markov model slightly underperforms-
668 the GFDL seasonal prediction system for cold season predictions using the previous-
669 summer observations in the Bering Sea, and for early summer predictions using-
670 previous early fall observations in the Sea of Okhotsk. It indicates that the weakness-
671 of the regional Markov model is mainly reflected in the SIE prediction using the-
672 previous late summer and early fall observations compared with the GFDL seasonal-
673 prediction system, which is likely because the surface climate anomaly in late-
674 summer/early fall loses its identity in fall and does not contribute to winter sea ice-
675 variability. Overall, the regional Markov model delivers skillful SIE predictions in
676 seasonal ice zones of the Pacific sector up to 76 month lead times, an improvement
677 from the 3 month leads displayed in the GFDL seasonal prediction system.

678 4.3 Sensitivity of model domain on the prediction skill

679 We conducted a sensitivity analysis of the model domain on prediction skills in
680 the Bering Sea and the Sea of Okhotsk with the same model configuration and
681 different sizes of the model domain. The model domain is defined by 90°E to 270°E,
682 120°E to 240°E and 135°E to 225°E respectively. The results show that the prediction
683 skill patterns based on three model domains show high similarity in the Bering Sea

684 and the skill based on the model domain (120°E to 240°E) is highest at all month
 685 leads. The prediction skill in the Sea of Okhotsk based on the model domain (135°E
 686 to 225°E) is highlighted at 5- to 8-month leads, but not well at 11- to 12-month leads.
 687 Although the models with different sizes of model domain have different prediction
 688 skills in the Bering Sea and the Sea of Okhotsk, the differences are not significant
 689 because all those model domains contain highly similar signals of climate variability.
 690 Therefore, the regional model is not highly sensitive to the size of the model domain
 691 within the Pacific-Arctic sector.



692
 693 **Figure 12.** Cross-validated model skills of the regional Markov model with the
 694 same model configuration and different sizes of the model domain. (a) The skills are
 695 measured by the ACC between predictions and observations with trends from 1980 to
 696 2020 as a function of lead months in the Bering Sea. (b) is the same as (a) except for
 697 the Sea of Okhotsk. The model is configured by V9M16 in winter, V11M20 in spring,
 698 V5M10 in summer, and V5M7 in autumn. The ACC values are averaged over the area
 699 marked in the black box in Figure 1.

700 **54** Conclusions

701 Here, we developed a regional Markov model to predict SIC in the Pacific-
702 Arctic sector at the seasonal time scale. The model was constructed in
703 the MEOF space so that the model can capture the covariability of the North Pacific
704 climate system defined by 97 variables (SIC, OHC, SIT, SST, SAT, surface net
705 radiative flux, surface net turbulent heat flux, and geopotential height and winds at
706 850 hPa). Based on cross-validation experiments, we selected model variables and
707 mode truncations that provided the best results in each season. These model
708 configurations were V97M165 for winter, V117M2043 for spring, V58M104 for
709 summer, and V58M79 for autumn. ~~The V7 models utilize SIC, SST, SAT, and surface~~
710 ~~net radiative flux as predictor variables, whereas the V8 models use SIC, SST, SAT,~~
711 ~~winds and geopotential height.~~

712 The SIC prediction skill was evaluated at each grid cell and for all seasons using
713 ACC. The regional Markov model's skill is superior to the skill derived from anomaly
714 persistence, revealing the model's ability to capture more predictable SIC internal
715 variability than anomaly persistence. The winter skill is about 0.4 in the Sea of
716 Okhotsk and 0.5 in the northern Bering Strait Sea at up to 12-month leads. The spring
717 prediction shows a similar pattern but with a 0.1 ~~increase~~reduction in the ACC skill.
718 The model skill in summer and autumn is more than 0.6 within the Arctic basin.
719 Compared with the pan-Arctic seasonal prediction model (Yuan et al., 2016), the
720 regional Markov model distinctly improves the SIC prediction skill in the peripheral
721 seas of the Pacific-Arctic sector. The regional model significantly
722 enhances the correlation skill from the pan-Arctic model for 42- to 12-month lead
723 predictions in the Bering Sea and 1- to 7-month lead predictions in the Sea of
724 Okhotsk. The improvement ~~measured by the PGS~~ is a 7532% ACC increase in the
725 Bering Sea and 186% in the Sea of Okhotsk. ~~The ACC is also increased by 21% in the~~
726 ~~Bering Sea and 8% in the Sea of Okhotsk.~~ In addition, similar to the pan-Arctic
727 Markov model, the regional model is not sensitive to the number of MEOF modes
728 retained, which indicates that the performance of this Markov model is robust.-

729 ~~Additionally, the regional Markov model's skill is superior to the skill derived from~~
730 ~~anomaly persistence, revealing the model's ability to capture more predictable SIC~~
731 ~~internal variability than anomaly persistence.~~

732 The model retains prediction skill ~~after regardless of whether the~~ sea ice trend is
733 removed or not. ~~H~~ However, the detrended skill is notably lower, consistent with
734 earlier sea ice prediction studies. When sea ice time series includes the trend, the
735 model ~~can skillfully predict~~ has good skill at predicting SIE from January to
736 November. The skill is particularly high for the predictions of summer and autumn
737 sea ice at longer lead times, especially in July to ~~November~~ October when the skill is
738 high (>0.6) even at ~~a~~ 9-12-month lead ~~months~~. ~~Conversely, in May, T~~ the model skill
739 is relatively low ~~in May and December~~, especially at ~~4-8-11~~ lead months. Trend
740 removal from ~~both~~ predictions and observations results in a ~~53~~ 35% reduction of the
741 mean ACC for the entire ~~Pacific-Arctic~~ Arctic-Pacific sector. However, the model only
742 reduces ~~13~~ 14% of the mean ACC from January to ~~November~~ October at 1-2 lead
743 months after the trend removal ~~for the North Pacific sector, including~~ in the Bering
744 Sea and the Sea of Okhotsk. This detrended analysis shows the model's capability of
745 capturing sea ice internal variability beyond linear trends. Furthermore, the regional
746 Markov model improves the detrended SIE prediction skill in the Pacific-~~Arctic~~ sector
747 to ~~7~~ 6 month lead times from the 3 month lead skill displayed in the GFDL-FLOR
748 seasonal prediction system.

749 The following reasons contribute to the improvements. First, the dominant climate
750 variability in the northern mid-high latitudes mostly occurs in the Atlantic sector of
751 the Arctic and subarctic, which dictates the leading MEOF mode in the pan-Arctic
752 model. The unique characteristics of atmosphere-ocean-sea ice coupled relationships
753 in the Pacific sector may not be included in the leading MEOF decompositions of the
754 pan-Arctic climate system and thus are not correctly represented in the model. The
755 regional model focuses on the Pacific-Arctic coupled atmosphere-ocean-sea ice
756 system and captures the dominant regional climate variability. Second, the Pacific
757 sector of the Arctic needs a different set of variables to maximize the model's

758 predictability. We added OHC and SIT in the regional model, which provides a
759 crucial source of predictability in winter and summer months respectively ~~surface net~~
760 ~~radiative flux, which partially controls the sea ice growth processes through its~~
761 ~~influences on the surface energy budget~~. We also include 850 hPa GPH and winds to
762 represent dynamic atmospheric processes in winter and include turbulent heat flux to
763 improve the model skill in spring. Finally, we constructed a superior model for each
764 season, isolating the seasonally dominant processes separately.

765 ~~The sensitivity experiments revealed that surface longwave radiation plays a~~
766 ~~significant role in the Pacific Arctic climate system variability in cold seasons when~~
767 ~~shortwave radiation is at its annual minimum. The 850 hPa GPH and winds mainly~~
768 ~~contribute to the model skill in warm seasons, reflecting that the influence of~~
769 ~~atmospheric circulation on sea ice is more easily captured by MEOF in warm seasons~~
770 ~~than in the cold season.~~ It was also found that more modes were needed in the cold
771 season to capture the predictable signal of SIC. This suggests that sea ice in cold
772 seasons has more variability patterns compared with that in warm seasons, which may
773 bring more errors in prediction. SIC trends are ~~also~~ strongest in the warm season
774 months, which may contribute to the smaller number of modes required. In addition to
775 the climate system in the Arctic Basin, the coupled atmosphere-ocean-sea ice
776 variability in the North Pacific plays a more important role in the cold season and
777 needs more modes to capture the covariability signals.—

778 ~~However, weaknesses of the model remain. The summer initialization months~~
779 ~~have little sea ice coverage, and SST does not provide enough memory for winter~~
780 ~~predictions in the Bering Sea and the Sea of Okhotsk due to shallow summer mixed~~
781 ~~layers. Thus, other sources of memory are required to provide sea ice prediction skill~~
782 ~~in cold seasons. By the mechanism for mid-latitude SST reemergence, subsurface~~
783 ~~ocean temperature anomalies in summer would potentially impact sea ice growth rates~~
784 ~~the following cold season~~ (Bushuk et al., 2017a; Bushuk et al., 2020). ~~These~~
785 ~~deficiencies provide us with opportunities for improvements in future work.~~

786

787 *Data availability.* The sea ice concentration data were obtained from the National
788 Snow and Ice Data Center (NSIDC, <https://nsidc.org/data/NSIDC-0079>, last access: 1
789 July 2021, Comiso, 2017). [Monthly SIT from the Pan-Arctic Ice-Ocean and](#)
790 [Assimilating System \(PIOMAS\) can be obtained from the Polar Science Center \(PSC\)](#)
791 [\(\[anomaly/data/model_grid\]\(http://psc.apl.uw.edu/research/projects/arctic-sea-ice-volume-
792 <a href=\), last access: 1 July 2021, Zhang and Rothrock, 2003\). The
793 \[ocean heat content in the upper 300 m\]\(#\), sea surface temperature, surface air
794 temperature, surface net radiative flux, surface net turbulent heat flux, 850_hPa
795 geopotential height, and 850_hPa wind vector from ~~the~~ ERA5 can be obtained from
796 the ECMWF \(<https://cds.climate.copernicus.eu/cdsapp#!/search?type=dataset>, last
797 access: 1 July 2021, Hersbach et al., 2020\).](http://psc.apl.uw.edu/research/projects/arctic-sea-ice-volume-)

798

799 *Supplement.* The supplement related to this article is available online at: **xxxx**.

800

801 *Author contributions.* YW, XY and HB conceived the idea for the protocol and
802 [experimental](#) design. MB and HH provided primary support and guidance on the
803 research. YW, YL and CL performed data processing. All authors drafted the
804 manuscript, and contributed to ~~the~~ manuscript revision.

805

806 *Competing interests.* The authors declare that they have no conflict of interest.

807

808 *Acknowledgements.* This work is supported by the Lamont endowment, the National
809 Natural Science Foundation of China (42106223), and the China Postdoctoral Science
810 Foundation (2020TQ0322). We thank the NSIDC for providing the sea ice
811 concentration data on their website (<https://nsidc.org/data/NSIDC-0079>). [Monthly](#)
812 [SIT from the Pan-Arctic Ice-Ocean and Assimilating System \(PIOMAS\) can be](#)
813 [obtained from the Polar Science Center \(PSC\)](#)
814 [\(\[anomaly/data/model_grid\]\(http://psc.apl.uw.edu/research/projects/arctic-sea-ice-volume-
815 <a href=\)\). The \[ocean heat content in the upper 300 m\]\(#\), sea surface](http://psc.apl.uw.edu/research/projects/arctic-sea-ice-volume-)

816 temperature, surface air temperature, surface net radiative flux, surface net turbulent
817 heat flux, 850_hPa geopotential height, and 850_hPa wind vector from ~~the~~ ERA5 can
818 be obtained from the ECMWF
819 (<https://cds.climate.copernicus.eu/cdsapp#!/search?type=dataset>).

820

821 *Financial support.* This work is supported by the Lamont endowment, the National
822 Natural Science Foundation of China (42106223; [42076185](#)), ~~and the Natural Science~~
823 [Foundation of Shandong Province, China \(ZR2021QD059\)](#), the China Postdoctoral
824 Science Foundation (2020TQ0322), [and the Open Funds for the Key Laboratory of](#)
825 [Marine Geology and Environment, Institute of Oceanology, Chinese Academy of](#)
826 [Sciences \(MGE2021KG15; MGE2020KG04\)](#).

827 Lamont contribution number xxxx.

828 **References**

829

- 830 Andersson, T. R., Hosking, J. S., Perez-Ortiz, M., Paige, B., Elliott, A., Russell, C., Law, S., Jones, D.
831 C., Wilkinson, J., Phillips, T., Byrne, J., Tietsche, S., Sarojini, B. B., Blanchard-
832 Wrigglesworth, E., Aksenov, Y., Downie, R., and Shuckburgh, E.: Seasonal Arctic sea ice
833 forecasting with probabilistic deep learning, *Nature Communications*, 12,
834 <https://doi.org/10.1038/s41467-021-25257-4>, 2021.
- 835 Barnston, A. G. and Ropelewski, C. F.: Prediction of ENSO Episodes Using Canonical Correlation
836 Analysis, *J. Clim.*, 5, 1316-1345, [https://doi.org/10.1175/1520-0442\(1992\)005<1316:poeuc>2.0.co;2](https://doi.org/10.1175/1520-0442(1992)005<1316:poeuc>2.0.co;2), 1992.
- 838 Blanchard-Wrigglesworth, E., Armour, K. C., Bitz, C. M., and DeWeaver, E.: Persistence and Inherent
839 Predictability of Arctic Sea Ice in a GCM Ensemble and Observations, *J. Clim.*, 24, 231-250,
840 <https://doi.org/10.1175/2010jcli3775.1>, 2011.
- 841 Blanchard-Wrigglesworth, E., Cullather, R., Wang, W., Zhang, J., and Bitz, C.: Model forecast skill
842 and sensitivity to initial conditions in the seasonal Sea Ice Outlook, *Geophys. Res. Lett.*, 42,
843 8042-8048, <https://doi.org/10.1002/2015GL065860>, 2015.
- 844 Blockley, E. W. and Peterson, K. A.: Improving Met Office seasonal predictions of Arctic sea ice using
845 assimilation of CryoSat-2 thickness, *Cryosphere*, 12, 3419-3438, <https://doi.org/10.5194/tc-12-3419-2018>, 2018.
- 847 Bushuk, M. and Giannakis, D.: The Seasonality and Interannual Variability of Arctic Sea Ice
848 Reemergence, *J. Clim.*, 30, 4657-4676, <https://doi.org/10.1175/jcli-d-16-0549.1>, 2017.
- 849 Bushuk, M., Msadek, R., Winton, M., Vecchi, G., Yang, X., Rosati, A., and Gudgel, R.: Regional
850 Arctic sea-ice prediction: potential versus operational seasonal forecast skill, *CIDy*, 52, 2721-
851 2743, <https://doi.org/10.1007/s00382-018-4288-y>, 2019.

852 Bushuk, M., Msadek, R., Winton, M., Vecchi, G. A., Gudgel, R., Rosati, A., and Yang, X.: Skillful
853 regional prediction of Arctic sea ice on seasonal timescales, *Geophys. Res. Lett.*, 44, 4953-
854 4964, <https://doi.org/10.1002/2017GL073155>, 2017a.

855 Bushuk, M., Msadek, R., Winton, M., Vecchi, G. A., Gudgel, R., Rosati, A., and Yang, X.: Summer
856 Enhancement of Arctic Sea Ice Volume Anomalies in the September-Ice Zone, *J. Clim.*, 30,
857 2341-2362, <https://doi.org/10.1175/jcli-d-16-0470.1>, 2017b.

858 Bushuk, M., Winton, M., Bonan, D. B., Blanchard-Wrigglesworth, E., and Delworth, T. L.: A
859 Mechanism for the Arctic Sea Ice Spring Predictability Barrier, *Geophys. Res. Lett.*, 47,
860 <https://doi.org/10.1029/2020gl088335>, 2020.

861 Bushuk, M., Winton, M., Haumann, F. A., Delworth, T., Lu, F., Zhang, Y., Jia, L., Zhang, L., Cooke,
862 W., Harrison, M., Hurlin, B., Johnson, N. C., Kapnick, S. B., McHugh, C., Murakami, H.,
863 Rosati, A., Tseng, K.-C., Wittenberg, A. T., Yang, X., and Zeng, F.: Seasonal Prediction and
864 Predictability of Regional Antarctic Sea Ice, *J. Clim.*, 34, 6207-6233,
865 <https://doi.org/10.1175/jcli-d-20-0965.1>, 2021.

866 Cañizares, R., Kaplan, A., Cane, M. A., Chen, D., and Zebiak, S. E.: Use of data assimilation via linear
867 low-order models for the initialization of El Niño–Southern Oscillation predictions, *Journal of*
868 *Geophysical Research: Oceans*, 106, 30947-30959, <https://doi.org/10.1029/2000JC000622>,
869 2001.

870 Chen, D. and Yuan, X.: A Markov model for seasonal forecast of Antarctic sea ice, *J. Clim.*, 17, 3156-
871 3168, [https://doi.org/10.1175/1520-0442\(2004\)017<3156:AMMFSF>2.0.CO;2](https://doi.org/10.1175/1520-0442(2004)017<3156:AMMFSF>2.0.CO;2), 2004.

872 Chen, T. C.: The structure and maintenance of stationary waves in the winter Northern Hemisphere,
873 *Journal of the Atmospheric Sciences*, 62, 3637-3660, <https://doi.org/10.1175/jas3566.1>, 2005.

874 Cheng, W., Blanchard-Wrigglesworth, E., Bitz, C. M., Ladd, C., and Stabeno, P. J.: Diagnostic sea ice
875 predictability in the pan-Arctic and US Arctic regional seas, *Geophys. Res. Lett.*, 43, 11688-
876 11696, <https://doi.org/10.1002/2016gl070735>, 2016.

877 Chi, J. and Kim, H.-c.: Prediction of Arctic Sea Ice Concentration Using a Fully Data Driven Deep
878 Neural Network, *Remote Sensing*, 9, <https://doi.org/10.3390/rs9121305>, 2017.

879 Cohen, J., Zhang, X., Francis, J., Jung, T., Kwok, R., Overland, J., Ballinger, T., Bhatt, U., Chen, H.,
880 and Coumou, D.: Divergent consensus on Arctic amplification influence on midlatitude
881 severe winter weather, *Nature Climate Change*, 10, 20-29, [https://doi.org/10.1038/s41558-](https://doi.org/10.1038/s41558-019-0662-y)
882 019-0662-y, 2020.

883 Comiso, J. C.: Bootstrap Sea Ice Concentrations from Nimbus-7 SMMR and DMSP SSM/I-SSMIS,
884 Version 3. NASA National Snow and Ice Data Center Distributed Active Archive Center,
885 Boulder, Colorado USA, 2017.

886 Dai, P., Gao, Y., Counillon, F., Wang, Y., Kimmritz, M., and Langehaug, H. R.: Seasonal to decadal
887 predictions of regional Arctic sea ice by assimilating sea surface temperature in the
888 Norwegian Climate Prediction Model, *CIDy*, 54, 3863-3878, [https://doi.org/10.1007/s00382-](https://doi.org/10.1007/s00382-020-05196-4)
889 020-05196-4, 2020.

890 Day, J. J., Hawkins, E., and Tietsche, S.: Will Arctic sea ice thickness initialization improve seasonal
891 forecast skill?, *Geophys. Res. Lett.*, 41, 7566-7575, <https://doi.org/10.1002/2014gl061694>,
892 2014a.

893 Day, J. J., Tietsche, S., and Hawkins, E.: Pan-Arctic and Regional Sea Ice Predictability: Initialization
894 Month Dependence, *J. Clim.*, 27, 4371-4390, <https://doi.org/10.1175/JCLI-D-13-00614.1>,
895 2014b.

896 Deser, C., Tomas, R., Alexander, M., and Lawrence, D.: The seasonal atmospheric response to
897 projected Arctic sea ice loss in the late twenty-first century, *J. Clim.*, 23, 333-351,
898 <https://doi.org/10.1175/2009JCLI3053.1>, 2010.

899 Francis, J. A. and Vavrus, S. J.: Evidence linking Arctic amplification to extreme weather in mid-
900 latitudes, *Geophys. Res. Lett.*, 39, <https://doi.org/10.1029/2012GL051000>, 2012.

901 Frankignoul, C., Sennechael, N., and Cauchy, P.: Observed Atmospheric Response to Cold Season Sea
902 Ice Variability in the Arctic, *J. Clim.*, 27, 1243-1254, [https://doi.org/10.1175/jcli-d-13-](https://doi.org/10.1175/jcli-d-13-00189.1)
903 00189.1, 2014.

904 Gregory, W., Tsamados, M., Stroeve, J., and Sollich, P.: Regional September Sea Ice Forecasting with
905 Complex Networks and Gaussian Processes, *Weather and Forecasting*, 35, 793-806,
906 <https://doi.org/10.1175/WAF-D-19-0107.1>, 2020.

907 Guemas, V., Blanchard-Wrigglesworth, E., Chevallier, M., Day, J. J., Déqué, M., Doblas-Reyes, F. J.,
908 Fučkar, N. S., Germe, A., Hawkins, E., and Keeley, S.: A review on Arctic sea-ice
909 predictability and prediction on seasonal to decadal time-scales, *QJRMS*, 142, 546-561,
910 <https://doi.org/10.1002/qj.2401>, 2016a.

911 Guemas, V., Chevallier, M., Deque, M., Bellprat, O., and Doblas-Reyes, F.: Impact of sea ice
912 initialization on sea ice and atmosphere prediction skill on seasonal timescales, *Geophys. Res.*
913 *Lett.*, 43, 3889-3896, <https://doi.org/10.1002/2015gl066626>, 2016b.

914 Hamilton, L. C. and Stroeve, J.: 400 predictions: The search sea ice outlook 2008–2015, *Polar Geogr.*,
915 39, 274-287, <https://doi.org/10.1080/1088937X.2016.1234518>, 2016.

916 Hersbach, H., Bell, B., Berrisford, P., Hirahara, S., Horányi, A., Muñoz-Sabater, J., Nicolas, J.,
917 Peubey, C., Radu, R., and Schepers, D.: The ERA5 global reanalysis, *QJRMS*, 146, 1999-
918 2049, <https://doi.org/10.1002/qj.3803>, 2020.

919 Horvath, S., Stroeve, J., and Rajagopalan, B.: A linear mixed effects model for seasonal forecasts of
920 Arctic sea ice retreat, *Polar Geogr.*, doi: 10.1080/1088937X.2021.1987999, 2021. 1-18,
921 <https://doi.org/10.1080/1088937X.2021.1987999>, 2021.

922 Horvath, S., Stroeve, J., Rajagopalan, B., and Kleiber, W.: A Bayesian Logistic Regression for
923 Probabilistic Forecasts of the Minimum September Arctic Sea Ice Cover, *Earth and Space*
924 *Science*, 7, <https://doi.org/10.1029/2020ea001176>, 2020.

925 Huang, Y., Dong, X., Xi, B., Dolinar, E. K., and Stanfield, R. E.: Quantifying the Uncertainties of
926 Reanalyzed Arctic Cloud and Radiation Properties using Satellite-surface Observations, *CIDy*,
927 30, 8007-8029, <https://doi.org/10.1175/JCLI-D-16-0722.1>, 2015.

928 Kapsch, M. L., Graverson, R. G., and Tjernström, M.: Springtime atmospheric energy transport and the
929 control of Arctic summer sea-ice extent, *Nature Climate Change*, 3, 744-748,
930 <https://doi.org/10.1038/nclimate1884>, 2013.

931 Kim, K.-Y., Hamlington, B. D., Na, H., and Kim, J.: Mechanism of seasonal Arctic sea ice evolution
932 and Arctic amplification, *The Cryosphere*, 10, 2191-2202, [https://doi.org/10.5194/tc-10-2191-](https://doi.org/10.5194/tc-10-2191-2016)
933 2016, 2016.

934 Kimmritz, M., Counillon, F., Smedsrud, L. H., Bethke, I., Keenlyside, N., Ogawa, F., and Wang, Y.:
935 Impact of Ocean and Sea Ice Initialisation On Seasonal Prediction Skill in the Arctic, *Journal*
936 *of Advances in Modeling Earth Systems*, 11, 4147-4166,
937 <https://doi.org/10.1029/2019ms001825>, 2019.

938 Koenigk, T., Caian, M., Nikulin, G., and Schimanke, S.: Regional Arctic sea ice variations as predictor
939 for winter climate conditions, *CIDy*, 46, 317-337, <https://doi.org/10.1007/s00382-015-2586-1>,
940 2016.

941 Lee, S., Gong, T., Feldstein, S. B., Screen, J. A., and Simmonds, I.: Revisiting the Cause of the 1989–
942 2009 Arctic Surface Warming Using the Surface Energy Budget: Downward Infrared
943 Radiation Dominates the Surface Fluxes, *Geophys. Res. Lett.*, 44, 10654-10661,
944 <https://doi.org/10.1002/2017GL075375>, 2017.

945 Lenetsky, J. E., Tremblay, B., Brunette, C., and Meneghello, G.: Subseasonal Predictability of Arctic
946 Ocean Sea Ice Conditions: Bering Strait and Ekman-Driven Ocean Heat Transport, *J. Clim.*,
947 34, 4449-4462, <https://doi.org/10.1175/jcli-d-20-0544.1>, 2021.

948 Lindsay, R., Zhang, J., Schweiger, A., and Steele, M.: Seasonal predictions of ice extent in the Arctic
949 Ocean, *Journal of Geophysical Research: Oceans*, 113,
950 <https://doi.org/10.1029/2007JC004259>, 2008.

951 Liu, Y. and Key, J. R.: Less winter cloud aids summer 2013 Arctic sea ice return from 2012 minimum,
952 *Environmental Research Letters*, 9, 044002, <https://doi.org/10.1088/1748-9326/9/4/044002>,
953 2014.

954 Luo, B., Luo, D., Wu, L., Zhong, L., and Simmonds, I.: Atmospheric circulation patterns which
955 promote winter Arctic sea ice decline, *Environmental Research Letters*, 12, 1-13,
956 <https://doi.org/10.1088/1748-9326/aa69d0>, 2017.

957 Meleshko, V., Kattsov, V., Mirvis, V., Baidin, A., Pavlova, T., and Govorkova, V.: Is there a link
958 between Arctic sea ice loss and increasing frequency of extremely cold winters in Eurasia and
959 North America? Synthesis of current research, *Russian Meteorology and Hydrology*, 43, 743-
960 755, <https://doi.org/10.3103/S1068373918110055>, 2018.

961 Morioka, Y., Iovino, D., Cipollone, A., Masina, S., and Behera, S.: Summertime sea-ice prediction in
962 the Weddell Sea improved by sea-ice thickness initialization, *Sci. Rep.*, 11,
963 <https://doi.org/10.1038/s41598-021-91042-4>, 2021.

964 Msadek, R., Vecchi, G. A., Winton, M., and Gudgel, R. G.: Importance of initial conditions in seasonal
965 predictions of Arctic sea ice extent, *Geophys. Res. Lett.*, 41, 5208-5215,
966 <https://doi.org/10.1002/2014gl060799>, 2014.

967 Peterson, A. K., Fer, I., McPhee, M. G., and Randelhoff, A.: Turbulent heat and momentum fluxes in
968 the upper ocean under Arctic sea ice, *Journal of Geophysical Research: Oceans*, 122, 1439-
969 1456, <https://doi.org/10.1002/2016JC012283>, 2017.

970 Peterson, K. A., Arribas, A., Hewitt, H., Keen, A., Lea, D., and McLaren, A.: Assessing the forecast
971 skill of Arctic sea ice extent in the GloSea4 seasonal prediction system, *CIDy*, 44, 147-162,
972 <https://doi.org/10.1007/s00382-014-2190-9>, 2015.

973 Petty, A., Schröder, D., Stroeve, J., Markus, T., Miller, J., Kurtz, N., Feltham, D., and Flocco, D.:
974 Skillful spring forecasts of September Arctic sea ice extent using passive microwave sea ice
975 observations, *Earth's Future*, 5, 254-263, <https://doi.org/10.1002/2016EF000495>, 2017.

976 Porter, D. F., Cassano, J. J., and Serreze, M. C.: Analysis of the Arctic atmospheric energy budget in
977 WRF: A comparison with reanalyses and satellite observations, *Journal of Geophysical
978 Research Atmospheres*, 116, <https://doi.org/10.1029/2011JD016622>, 2011.

979 Sévellec, F., Fedorov, A. V., and Liu, W.: Arctic sea-ice decline weakens the Atlantic meridional
980 overturning circulation, *Nature Climate Change*, 7, 604-610,
981 <https://doi.org/10.1038/NCLIMATE3353>, 2017.

982 Schweiger, A., Lindsay, R., Zhang, J., Steele, M., Stern, H., and Kwok, R.: Uncertainty in modeled
983 Arctic sea ice volume, *Journal of Geophysical Research-Oceans*, 116,
984 <https://doi.org/10.1029/2011jc007084>, 2011.

985 Screen, J. A. and Francis, J. A.: Contribution of sea-ice loss to Arctic amplification is regulated by
986 Pacific Ocean decadal variability, *Nature Climate Change*, 6, 856-860,
987 <https://doi.org/10.1038/NCLIMATE3011>, 2016.

988 Screen, J. A., Simmonds, I., Deser, C., and Tomas, R.: The atmospheric response to three decades of
989 observed Arctic sea ice loss, *J. Clim.*, 26, 1230-1248, [https://doi.org/10.1175/JCLI-D-12-](https://doi.org/10.1175/JCLI-D-12-00063.1)
990 00063.1, 2013.

991 Sigmond, M., Fyfe, J. C., Flato, G. M., Kharin, V. V., and Merryfield, W. J.: Seasonal forecast skill of
992 Arctic sea ice area in a dynamical forecast system, *Geophys. Res. Lett.*, 40, 529-534,
993 <https://doi.org/10.1002/grl.50129>, 2013.

994 Smith, D. M., Dunstone, N. J., Scaife, A. A., Fiedler, E. K., Copsey, D., and Hardiman, S. C.:
995 Atmospheric response to Arctic and Antarctic sea ice: The importance of ocean-atmosphere
996 coupling and the background state, *J. Clim.*, 30, 4547-4565, [https://doi.org/10.1175/JCLI-D-](https://doi.org/10.1175/JCLI-D-18-0100.1)
997 18-0100.1, 2017.

998 Smith, L. C. and Stephenson, S. R.: New Trans-Arctic shipping routes navigable by midcentury,
999 *Proceedings of the National Academy of Sciences*, 110, E1191-E1195,
1000 <https://doi.org/10.1073/pnas.1214212110>, 2013.

1001 Swart, N.: Natural causes of Arctic sea-ice loss, *Nature Climate Change*, 7, 239-241,
1002 <https://doi.org/10.1038/nclimate3254>, 2017.

1003 Tian, T., Yang, S., Karami, M. P., Massonnet, F., Kruschke, T., and Koenigk, T.: Benefits of sea ice
1004 initialization for the interannual-to-decadal climate prediction skill in the Arctic in EC-Earth3,
1005 *Geoscientific Model Development*, 14, 4283-4305, [https://doi.org/10.5194/gmd-14-4283-](https://doi.org/10.5194/gmd-14-4283-2021)
1006 2021, 2021.

1007 Ting, M. F.: MAINTENANCE OF NORTHERN SUMMER STATIONARY WAVES IN A GCM,
1008 *Journal of the Atmospheric Sciences*, 51, 3286-3308, [https://doi.org/10.1175/1520-](https://doi.org/10.1175/1520-0469(1994)051<3286:monssw>2.0.co;2)
1009 0469(1994)051<3286:monssw>2.0.co;2, 1994.

1010 Wang, L., Scott, K. A., and Clausi, D. A.: Sea ice concentration estimation during freeze-up from SAR
1011 imagery using a convolutional neural network, *Remote Sensing*, 9, 408,
1012 <https://doi.org/10.3390/rs9050408>, 2017.

1013 Wang, L., Yuan, X., and Li, C.: Subseasonal forecast of Arctic sea ice concentration via statistical
1014 approaches, *CIJy*, 52, 4953-4971, <https://doi.org/10.1007/s00382-018-4426-6>, 2019a.

1015 Wang, L., Yuan, X., Ting, M., and Li, C.: Predicting summer Arctic sea ice concentration intraseasonal
1016 variability using a vector autoregressive model, *J. Clim.*, 29, 1529-1543,
1017 <https://doi.org/10.1175/JCLI-D-15-0313.1>, 2016.

1018 Wang, Y., Yuan, X., Bi, H., Liang, Y., Huang, H., Zhang, Z., and Liu, Y.: The Contributions of Winter
1019 Cloud Anomalies in 2011 to the Summer Sea-Ice Rebound in 2012 in the Antarctic, *Journal*
1020 *of Geophysical Research: Atmospheres*, 124, 3435-3447,
1021 <https://doi.org/10.1029/2018JD029435>, 2019b.

1022 Wu, B., Wang, J., and Walsh, J. E.: Dipole Anomaly in the Winter Arctic Atmosphere and Its
1023 Association with Sea Ice Motion, *J. Clim.*, 19, 210-225, <https://doi.org/10.1175/JCLI3619.1>,
1024 2006.

1025 Wu, Q., Cheng, L., Chan, D., Yao, Y., Hu, H., and Yao, Y.: Suppressed midlatitude summer
1026 atmospheric warming by Arctic sea ice loss during 1979–2012, *Geophys. Res. Lett.*, 43, 2792-
1027 2800, <https://doi.org/10.1002/2016GL068059>, 2016.

1028 Wu, Q., Yan, Y., and Chen, D.: A linear Markov model for East Asian monsoon seasonal forecast, *J.*
1029 *Clim.*, 26, 5183-5195, <https://doi.org/10.1175/JCLI-D-12-00408.1>, 2013.

1030 Xie, J., Counillon, F., Bertino, L., Tian-Kunze, X., and Kaleschke, L.: Benefits of assimilating thin sea
1031 ice thickness from SMOS into the TOPAZ system, *Cryosphere*, 10, 2745-2761,
1032 <https://doi.org/10.5194/tc-10-2745-2016>, 2016.

1033 Xue, Y., Leetmaa, A., and Ji, M.: ENSO prediction with Markov models: The impact of sea level, *J.*
1034 *Clim.*, 13, 849-871, [https://doi.org/10.1175/1520-0442\(2000\)013](https://doi.org/10.1175/1520-0442(2000)013), 2000.

1035 Yuan, X., Chen, D., Li, C., Wang, L., and Wang, W.: Arctic sea ice seasonal prediction by a linear
1036 Markov model, *J. Clim.*, 29, 8151-8173, <https://doi.org/10.1175/JCLI-D-15-0858.1>, 2016.

1037 Zhang, J. L. and Rothrock, D. A.: Modeling global sea ice with a thickness and enthalpy distribution
1038 model in generalized curvilinear coordinates, *MWRv*, 131, 845-861,
1039 [https://doi.org/10.1175/1520-0493\(2003\)131<0845:mgsiwa>2.0.co;2](https://doi.org/10.1175/1520-0493(2003)131<0845:mgsiwa>2.0.co;2), 2003.

1040 Zuo, H., Balmaseda, M. A., Tietsche, S., Mogensen, K., and Mayer, M.: The ECMWF operational
1041 ensemble reanalysis-analysis system for ocean and sea ice: a description of the system and
1042 assessment, *Ocean Sci.*, 15, 779-808, <https://doi.org/10.5194/os-15-779-2019>, 2019.

1043